DEGREE PROJECT, IN ENGINEERING PHYSICS , SECOND LEVEL
STOCKHOLM, *SWEDEN 2015*

Modeling the Effects of Strain in Multiferroic Manganese Perovskites

MARKUS SILBERSTEIN HONT

KTH ROYAL INSTITUTE OF TECHNOLOGY

SCHOOL OF INFORMATION AND COMMUNICATION TECHNOLOGY

Abstract

The effects of strain on the magnetic phases in perovskites are of interest in the highly active research field of multiferroics. A Monte Carlo program is written to investigate the influence of strain on the low–temperature magnetic phase diagram of the manganese perovskites, $R\mathrm{MnO}_3$, where R is a cation in the lanthanide series. A Metropolis simulation scheme is implemented together with parallel tempering to perform computations in a two–dimensional geometry using a conventional nearest–neighbor and next–nearest–neighbor Heisenberg Hamiltonian, extended to include spin–lattice couplings and single–ion anisotropies. The latter two are important to account for structural distortions such as octahedral tilting and the Jahn–Teller effect. It is shown that even weak single–ion anisotropies render incommensurability in the otherwise structurally commensurate E–type ordering, and that the Dzyaloshinskii–Moriya interaction, in combination with single–ion anisotropies, is crucial for the stabilization of previously experimentally observed incommensurate spin spirals. Simulations performed to account for strain in the crystallographic ab–plane show that tensile strain may improve stability of E–type ordering for R elements with small atomic radii and that compressive strain drives the magnetic ordering toward the incommensurate spiral states.

Keywords: Condensed matter physics, multiferroics, magnetism, spin modeling, computational physics

Sammanfattning

Modellering av spänningsinverkan på multiferroiska manganitperovskiter

Spänningsinverkan på de magnetiska faserna i perovskiter är av intresse inom den just nu högaktiva forskningen om multiferroiska material. Ett Monte Carlo-program har skrivits för att undersöka effekterna av spänning på de magnetiska lågtemperaturfaserna i multiferroiska manganitperovskiter, $R\mathrm{MnO}_3$, där R är en katjon i lantanoidserien. En kombination av Metropolisalgoritmen och parallelltemperering har använts för att utföra beräkningar i tvådimensionell geometri med en konventionell Heisenberghamiltonian, utökad till att även inkludera spinn–gitterkopplingar och enkeljonsanisotropier. De senare har visats vara viktiga för att ta i beaktande den strukturella distortion i materialet som följer av t.ex. syreoktahederförskjutning och Jahn–Tellereffekten. Det visas att även svaga anisotropier orsakar inkommensurabilitet i den i övrigt kommensurabla E–typsfasen, och att Dzyaloshinskii–Moriyainteraktionen, i kombination med anisotropitermerna, är avgörande för att kunna stabilisera de sedan tidigare experimentellt bekräftade inkommensurabla spinnspiralsfaserna. Simuleringar som modellerar spänning i materialets kristallografiska ab–plan visar att dragspänning kan förbättra stabiliteten hos E–typsfasen för R–atomer med liten radie och att tryckspänning leder den magnetiska ordningen mot inkommensurabla spiraltillstånd.

Nyckelord: Kondenserade materiens fysik, multiferroiska material, magnetism, spinnmodellering, beräkningsfysik

Acknowledgements

I would like to thank all members of Prof. Anna Delin's group at the Department of Materials and Nano Physics at KTH for welcoming me into their stimulating learning environment. I give special thanks and appreciation to my thesis supervisor, Dr. Johan Hellsvik, whose support, knowledge and commitment have been invaluable to me throughout the whole process, from diffuse brainchild to finished work. Also, I would like to extend my gratitude toward Dr. Pavel Bessarab for interesting discussions on Landau theory and for showing sincere interest in my work, and to Olof Bergvall at the Department of Mathematics at Stockholm University for taking time helping me grasp the fundamental concepts of representation theory.

Contents

Chapter 1

Introduction

Modern science has long relied on two main approaches, working in tandem. Theoreticians construct models which seek to describe natural phenomena. Experimentalists then develop ways of assessing the accuracy of the models, by means of controlled observation. (The reverse is, of course, equally valid.) In recent decades, however, and owing to the immense development of computational capability, there has been a rapid rise of numerical methods as a third approach to science, complementing the better–established previous two. Computerized models continue to serve as valuable tools when attempting to reject or confirm theoretical results where experiments are either unreliable or even unfeasible.

The thesis work presented here makes use of computational methods in the highly active research field of *multiferroics*, in which the magnetic phase diagram and ordered symmetries of the material play imperative roles. The objective has been to as accurately as possible reproduce quite recent experimental results from works on the effects of strain in the *perovskite* lattice structure, see e.g. [1, 2]. In doing this, there arises a possibility for predicting other results within the same class of problems which may not yet have been tested experimentally.

1.1 Multiferroics

The term multiferroics was coined by Schmid [3] and it refers to classes of materials which show simultaneously more than one ferroic order parameter which sometimes couple strongly with each other. Examples of four common ferroic order parameters are:

- **Ferroelasticity** – Materials exhibiting spontaneous strain
- **Ferroelectricity** – Materials exhibiting spontaneous electric polarization
- **Ferromagnetism** – Materials exhibiting spontaneous magnetization. This generalizes to include *antiferromagnetism* as well (Section 2.1.1).
- **Ferrotoroidicity** – Materials with vortices of magnetic moments. These vortices are also referred to as *skyrmions*.

A key aspect of ferroic order is that it is intimately related to their invariance (or lack thereof) under symmetry operations of space and time. This aspect is discussed in detail in Appendix B. Table 1.1, however, summarizes the main order parameters and their properties under space and time symmetry operations [4, 5].

It was first stipulated by Pierre Curie [6] in the late 19^{th} century and later in the 1950s by Landau and Lifshitz [7] that materials with multiferroic properties were possible, but it was not until much

Table 1.1: Ferroic order parameters and their invariance under space and time symmetry operations [4].

Time \ Space	**Invariant**	**Non–invariant**
Invariant	Ferroelasticity	Ferroelectricity
Non–invariant	Ferromagnetism	Ferrotoroidicity

later that their existence was confirmed experimentally. The fact that electricity and magnetism are intimately connected has been known since the 19^{th} century and has been described ever since using the theoretical framework of Maxwell. In materials science, however, the origins of these two phenomena have been studied separately [5]. This is because electric and magnetic polarization stem from two different sources: Electric polarization is caused by the spatial displacement of electric charges (something which may be caused by a range of phenomena) while the magnetic equivalent is caused by the time-resolved displacements of electrons (which are strongly connected to atom spins) [8]. But with Landau and Lifshitz came the birth of the field of multiferroics.

This thesis will concentrate on multiferroic materials showing magnetic and ferroelectric order simultaneously. Khomskii [8] defines two kinds of such multiferroic materials, which differ in that their ferroic order parameters couple to each other to varying extent. In a Type–I material, ferroelectricity and magnetism do not cause each other, and couple very weakly. A type–II material, on the other hand, has strong coupling between the two; Magnetic order will cause ferroelectricity. The latter is a quite recent discovery, made in 2003 [6] and since then the Type–II multiferroics have been a matter of highly active research.

1.2 Perovskites

One of the classes of materials which have been shown to possess Type–II multiferroicity are the magnetic perovskites. Their chemical formulas can be abbreviated by RBO_3, where R and B are cations. In this thesis work, the B element considered will always be Mn, and the associated class of perovskites is thus called *manganese perovskites* or *perovskite manganites*. The R element is most often a lanthanide (R = La–Lu). The structure is described by the orthorombic crystallographic group *Pnma* (No. 62), which is illustrated in Fig. 1.1. It consists of a body–centered Mn atom which has a non–zero atom spin (and hence also a non–zero localized magnetic moment) and is, together with non–zero exchange couplings, the direct cause of magnetic ordering at low temperatures [5]. In face–centered positions are oxygen atoms which form an octahedral cage–like shape around the Mn. In the simple–rectangular corners are the R atoms. The oxygen atoms and their interactions with the R and Mn elements contribute – indirectly but to a great extent – to the characteristics of the magnetic phase diagram of the perovskite structure. This will be discussed in greater detail in Sections 2.3.1 and 2.3.3.

Manganese perovskites were the first multiferroic materials of this kind to be discovered, and it was found that they made possible an *improper* polarization, i.e. its ferroelectric order is initiated by magnetic ordering (hence making it a Type–II multiferroic) as opposed to *proper* ferroelectricity in which the polarization is initated by broken inversion symmetry in the crystal structure itself [6, 9]. Due to this fact, the resultant ferroelectric polarization can potentially be switched on and off by controlling the magnetic ordering, something which is possible, for instance, via field gradients, temperature regulation or local laser pulse excitations – an ongoing field of research [10]. Applications to this feature exist, for example, in tentative spintronic devices which are among the technologies expected to enter the market in the "more than Moore" sense [11].

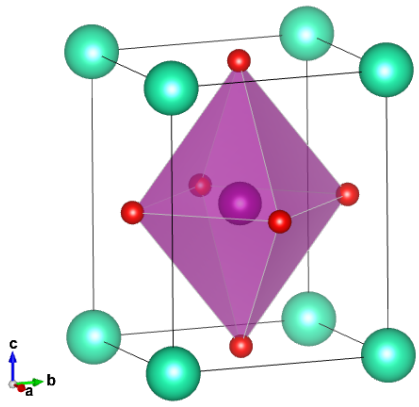

Figure 1.1: The $R\mathrm{MnO_3}$ perovskite structure. R, Mn and O atoms are colored green, purple and red, respectively. The shaded surface illustrates the oxygen octahedron structure.

Ferroelectric effects in perovskites appear as a consequence of certain kinds of magnetic ordering, the specific configurations of which make possible an electric polarization (see section 2.1). Knowledge of the magnetic phase diagram and its susceptibility to disorder and other defects that may be present is therefore of great interest. One such kind of disorder which is important in nanostructure physics in general (and certainly applies to perovskites in particular) is *geometric strain*. For real applications, being able to predict the phase diagram of a perovskite structure under the influence of strain is imperative to operation stability.

1.3 Problem Formulation and Motivation

Among recent experimental works are those conducted by Windsor [2]. In it the effects of strain in $\mathrm{LuMnO_3}$ thin films are described and the results reported there are the main targets for further investigation in this thesis work. The aim is to reproduce the results reported in this work, but by means of theoretical investigation.

Primarily, a Metropolis Monte Carlo program is written which uses a Heisenberg description to model the spin interactions within the manganese perovskite structure, in spirit of the extensive works of Mochizuki [9, 12], which models the phase diagrams of the undistorted lattice structure. Simulations will first be performed with these works as targets, and then the model will be extended so as to account for the effects of strain, and results in, for instance, [2] will be targeted.

In addition, the magnetic phase transitions can be studied further using Landau theory. Monte Carlo simulations are quasi–dynamic in the sense that, while performed at equilibrium, one usually studies the system for a discrete range of temperatures within which phase transitions are expected to take place. Because of the discreteness of the temperature mesh, it is not evident in all cases whether a phase transition can be considered first or second order [13]. The Landau theory may complement the simulations in this aspect. It is phenomenological, and if applied with sufficient rigor it is able to predict the order of the phase transitions. In the scope of this work, the theoretical framework is studied: An introduction is given to the theory and methods for the analyses are presented.

1.3.1 Benefits, Ethics and Sustainability

As mentioned in Section 1.2, improper ferroelectrics such as the manganese perovskites have potential to become important in the future of information technology. Binary information may be stored in magnetic domains in which, for instance, a nonzero net magnetization could correspond to a '1' state and zero net magnetization could represent a '0' state. Now, not only does this make for faster electronics since spin waves can propagate rather quickly through a lattice, but it is also interesting since transitions between states can be made at low energy costs [14]. This is an important motivation for the present study and works alike.

In real–life applications, strain is an important factor to take into account. For instance, an epitaxially grown thin film may experience different amounts of strain depending on the lattice mismatch between film and substrate, something which will have substantial effect on the magnetic phases in the film [2, 15]. Therefore, being able to accurately predict how strain will influence a material is important for controlling its fabrication (and any components made from it). To this end, theoretical investigations such as the present are valuable; Provided the theoretical model is accurate enough, there is no need for actual synthesis of any material, something which could potentially be quite inefficient and expensive in many cases. Rather, simulations can be safely and efficiently performed in large volumes and with quick modifications in between simulation runs, something which is beneficial because feedback may come faster than when synthesizing the real material. Also, results from simulations which are known to match existing experimental results may be extended so as to predict future results for slighlty different experimental settings.

Furthermore, fabrication of functional materials is in many cases a dangerous activity. Not seldom are toxic fumes involved, which are not only hazardous to the fabricator, but are also often harmful for the environment. Therefore, any limits that can be put to these kinds of emissions are beneficial, and thus simulations can serve as valuable alternatives.

1.4 Layout of Report

The rest of this thesis report is structured as follows. In section 2, summaries are given of fundamental concepts that are important for the remainder of this work. The theory of magnetic phase transitions is outlined (2.1), and the real physical phenomena which contribute to the magnetic characteristics of the structure (2.3) are discussed. Section 3 describes the computer model used in this work. Firstly, the Heisenberg model is discussed (3.1). Secondly, the Monte Carlo implementation of the model is presented (3.2). Section 4 presents the results and the discussion. Section 5 gives a brief summary and presents the conclusions. The fundamentals of magnetic groups and corepresentations are presented in Appendix A, which are later applied in the discussion of Landau theory in Appendix B.

Chapter 2

Background

Constructing a credible computer model requires a few important considerations. Firstly, the complexity of the model must be reasonable. It could not be too extensive because computer resources are limited. But also, one cannot use all too crude model assumptions because naturally it will lead to poor results. One of the main challenges is modeling the system in such a way that these limiting factors are held at a minimum.

In addition to these mere practical aspects, keeping up to date with recent progress in theoretical and experimental works is imperative to being able to accurately describe the real world using numerical modeling. If, as mentioned earlier, a computerized model is to overbridge theory and experiment, then an exhausting treatment of the one must be done in order to numerically simulate the other. This chapter discusses the fundamentals of existing theoretical descriptions of the perovskite structure and its magnetic phases.

2.1 Magnetic Phases and Phase Transitions

Microscopic interactions between atoms with nonzero magnetic moments may give rise to long–range magnetic ordering. The study of magnetic phases is at the heart of understanding multiferroic materials. This section introduces some key concepts and definitions and their connection to perovskite manganites.

2.1.1 Magnetic Ordering

In the simplest description, magnetic order can be separated into three categories. Disorder, i.e. purely random alignment of magnetic moments, is called *paramagnetism* (PM). When the spins favor being aligned with each other, the ordering is referred to as *ferromagnetic* (FM). When anti–alignment is favored, the ordering is *antiferromagnetic* (AFM) [16]. While the distinction between FM and AFM is an important one to make, further classification is necessary; Generally, structures will show ferromagnetic ordering in some crystallographic directions and antiferromagnetic ordering in others. Naming conventions used below are in spirit of Wollan and Koehler [17].

In perovskite manganites, there have been reports of four main types of ordering [1, 2, 5, 9]. At high temperatures (but low enough for magnetic ordering to be possible), a *sinusoidal collinear* phase is favored, in which the b–axis component is modulated sinusoidally (top of Fig. 2.1(b)). At even lower temperatures, the amount of structural distortion influences greatly the phases which can be realized (see Sections A and 2.3). For small distortions, when R is an element of larger atomic radius, the low–temperature phase is *A–type*, which essentially is FM in the *ab*–planes and has AFM–ordering in–between crystallographic planes (Fig. 2.1(a)). As the distortion

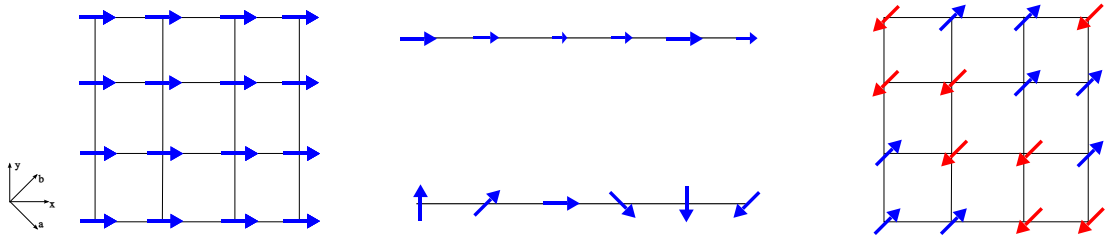

(a) A–type

(b) Sinusoidal collinear (top) and spin–spiral (bottom)

(c) E–type

Figure 2.1: Possible magnetic phases in perovskite manganites in the *ab*–plane.

increases, the low–temperature phase changes into a *spin–spiral* phase in which the spin directions are subject to *incommensurate modulation* (that is, a mismatch between the wave vector and the lattice periodicity). These spirals can be either in the *ab*– or *bc*–planes – see the bottom of Fig. 2.1(b).

For an even smaller R atom, or, equivalently, even larger distortions, the low–temperature phase is of *E–type* (Fig. 2.1(c)). It is highly important in the context of multiferroics, since the structure enables an unusually high resulting ferroelectric polarization [1, 9]. The E–type phase is subject for meticulous study in this thesis work. For some manganese perovskites, such as $LuMnO_3$ for instance, the low–temperature phase has been observed to be pure E–type, but for other, larger R elements, there are reports of an E–type phase in coexistence with an incommensurate spin spiral [9]. This complicates the study somewhat, but is indeed an interesting feature because this incommensurability in the E–type phase has been shown to feature different sources of the resulting ferroelectric polarization than the purely E–type phase [9]. This is explained by the fact that there are two kinds of contributions to the ferroelectric polarization, $\mathbf{P}$. The first is of $(\mathbf{S}\cdot\mathbf{S})$–type, where $\mathbf{S}$ is a spin vector, and this is the major contribution to $\mathbf{P}$ in the commensurate E–type structure. But there is also a possible $(\mathbf{S}\times\mathbf{S})$–type contribution to $\mathbf{P}$, which enters when the pure E–type phase is subjected to incommensurate modulation, as is the case in the observed coexistent state.

2.1.2 Magnetic Phase Transitions

The critical phenomena associated with letting the structure go from one type of magnetic ordering to another are of interest. A phase transition can be described using *order parameters*, a quantity which one is rather free to design depending on the context. The idea of the order parameter is to have it describe the symmetry of one phase and observe what happens to its value as one approaches a new phase (in which, preferably, it becomes zero). An example of an order parameter is the average magnetic moment of the sinusoidal phase described in the previous section. It can be described as $\mathbf{m}(\mathbf{r}_b) = \mathbf{m}_0 \exp(i\mathbf{k}\cdot\mathbf{r_b})$, where $\mathbf{r}_b$ is along the b–axis. When the system goes from the sinusoidal to the PM phase, the average magnetic moment becomes zero. In general, one distinguishes between two cases depending on whether this transition is continuous or not [16, 18]:

- A *first–order* phase transition is such that the order parameter experiences a discontinuous jump at the transition point.
- In a *second–order* phase transition, the order parameter goes to zero continuously.

A widely used framework for theoretically characterizing the nature of phase transitions is Landau theory, which in essence studies the approximate equilibrium free energy around the point of transition. This topic is discussed in greater detail in Appendix B.

2.2 Lattice Structure: Symmetry Considerations

Crystals are ordered structures. Thus, in addition to only specifying the locations of the atoms of a unit cell, they are aptly described by the symmetries under which they are invariant. The most basic example would be the simple–cubic lattice. It has one atom in its primitive unit cell. But also, it is invariant under rotations by $\frac{\pi}{2}$ about the principal axes and under mirroring in the planes spanned by the principal axes, to name a few examples. The complete set of symmetry operations describing the structure can be treated using the theoretical framework of group theory. We define the *point group* as being the collective set of symmetry operations which leaves the unit cell invariant. In addition, due to the fact that crystals are (ideally) infinite structures, one must also take into account the invariant translations of the lattice. The point group and the group of translations jointly constitute the *space group* of the structure [19].

The rigorous mathematical framework for describing the geometric (and magnetic) symmetries in a lattice relies upon representation theory. Using these concepts from abstract algebra, the most important aspects can be characterized, and the fundamentals of this theory are outlined in Appendix A. Furthermore, one is able to predict the different low–temperature magnetic phases that can possibly appear, given some paramagnetic lattice structure, and the natures of the transitions between these phases are also deductable. The framework for doing this is Landau theory, and its fundamentals are described in Appendix B.

2.3 Lattice Structure: Effects of Distortions

The unit cell shown in Fig. 1.1 is quite schematic. In reality, the structure will be distorted to different extents depending on a number of different physical effects. For instance, the cage–like structure formed by oxygen atoms around the Mn atoms can in fact be contracted and/or elongated along the principal axes owing to the *Jahn–Teller effect* described in Section 2.3.1. Also, they can be tilted and rotated in relation to each other as a consequence of interactions between the R element and the O atoms, as described in Section 2.3.2. Figure 2.2 shows a schematic of how the distorted structure might look.

These different kinds of distortions will have substantial effects on the magnetic phase diagram of the manganese perovskites. An important framework for describing this is the concept of *superexchange* which is discussed in Section 2.3.3.

2.3.1 The Jahn–Teller Effect

The Jahn–Teller (JT) effect is an example of electron–phonon coupling, which means that the interactions between electrons in the structure will affect the ions (and hence also the phonon modes). In essence, the JT theorem says that whenever a molecular configuration experiences an electronic degeneracy, the system will (almost always) strive toward lifting the degeneracy mainly by introducing structurally symmetry–breaking distortions [20, 21]. This holds true for most systems, albeit with a few exceptions. The perovskite structure, however, is not one of these [22].

The description of the JT effect builds upon the Born–Oppenheimer approximation [20], which supposes that the wavefunctions of electrons and nuclei of a system are uncoupled. Generally,

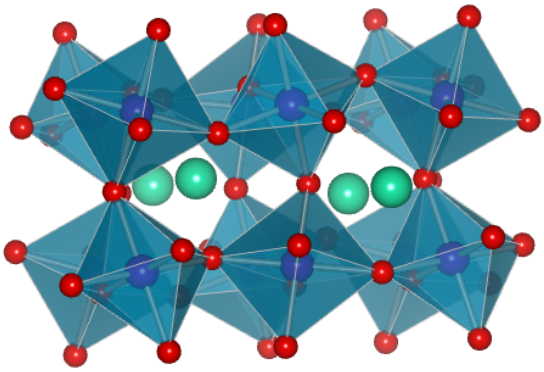

Figure 2.2: The distorted $R\mathrm{MnO_3}$ structure. Here, R, Mn and O atoms are colored green, purple and red, respectively.

the JT effect can be described as a perturbative correction to the Hamiltonian of the degenerate system:

$$\mathcal{H} = \mathcal{H}_0 + k\mathcal{H}_{\mathrm{JT}}, \tag{2.1}$$

where k is a correction coefficient called the JT parameter. The form of $\mathcal{H}_{\mathrm{JT}}$ will of course depend on the symmetry of the structure and it can be of different order in parameter space depending on the order of correction to the electron–phonon interaction that one wishes to include in the study [21]. Irregardless of the form, however, the minima of the Hamiltonian (2.1) will include modes which reflect the JT distortion.

In the perovskite structure, there is an overlap in the d–orbitals of the Mn and O atoms. Particularly, both the t_{2g} and e_g orbitals (Fig. 2.3) contribute to the degeneracy. In the symmetry of the perovskite structure, there are two competing vibrational modes, which act together to lift the degeneracy by shifting the O atoms away from their centered positions in between their neighboring Mn atoms, thus creating an anisotropic coupling [21, 23].

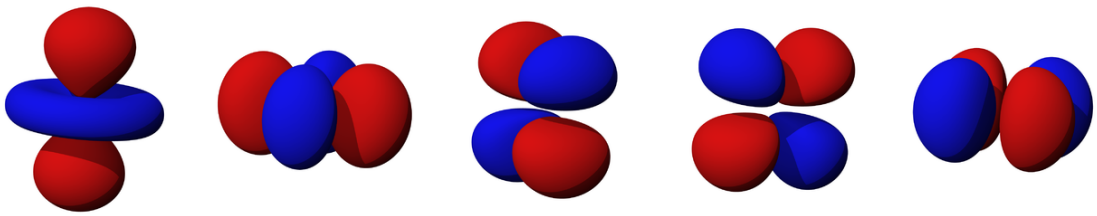

(a) d_{z^2} (b) $d_{x^2-y^2}$ (c) d_{xz} (d) d_{yz} (e) d_{yz}

Figure 2.3: The e_g ((a) and (b)) and t_{2g} ((c), (d) and (e)) orbitals.

2.3.2 Octahedral Tilting

The octahedral shape formed around the Mn atom by the O atoms in Figs. 1.1 and 2.2 will be tilted by different amounts depending on the stoichiometric formula of the perovskite structure.

Now, since the only variable element in the $R\mathrm{MnO}_3$ manganese perovskite is R, one is lead to believe that it is responsible for the differentiation between different $R\mathrm{MnO}_3$ molecules [9].

Generally, the octahedral tilting depends on the symmetry formed by the distorted structure; The new configuration (which necessarily is of lower symmetry) must be a subgroup of the symmetry group of the ideal structure [21]. In his work, Woodward [24] studies 23 potentially allowable tilt systems and concludes that, while many systems allow for pure tilted distortions, there are configurations which require structural distortions of the octahedrons themselves in order to retain a three–dimensional network of connected cages. Such distortions are equivalent to the JT effect described in the previous section.

Phenomenologically, the tilting changes the *coordination sphere*, i.e. the geometrical pattern of bonds to the central atom, about the R atom, while it is left unchanged about the Mn atom (again, see Fig. 2.2). Hence, it is indeed the case to a first approximation that octahedral tilting is driven by the configuration of anions around R [25]. It is shown in [25] that both the atomic radius as well as the charge of the R atom makes substantial difference in determining which tilting geometry will actually take form. Firstly, in regard to the atomic radius, one can define a tolerance factor as follows:

$$t = \frac{r_R + r_O}{2^{1/2}\,(r_{\mathrm{Mn}} + r_O)}, \tag{2.2}$$

where r_i is the (average) radius of atom i. It is shown that perovskite compounds exist in the range $1.05 > t > 0.78$ and depending on t, different tilt systems will be realized. Secondly, in regards to the charge of the R atom, it is seen that, owing to the large difference in ionic charge between O anions and R cations, the bonds will be largely ionic. The tilting structure realized then depends on the ratio between the R–O bonds and the ion repulsion between the R atoms themselves.

2.3.3 Superexchange and the Goodenough–Kanamori Rules

The physical effects described in the two previous subsections will mainly affect the positions of the O atoms in relation to the R and Mn atoms. In the manganese perovskite structure, it is the Mn atoms which have nonzero atom spins and hence also localized magnetic moments. The magnetic structure depends on the interactions between the Mn atom spins (see Section 2.1). Now, since there are no pure Mn–Mn bonds of significance in perovskites, these interactions will be strongly dependent on the Mn–O–Mn bonds which exist predominantly instead. In the Mn–O–Mn configuration, the interacting valence electrons are in the d, p and d orbitals, respectively. Thus, the interaction cannot be described by direct hopping of electrons between the Mn atoms [26]. Instead, the interaction must take place via the O atom. This kind of interactions between magnetic cations through an intermediate (non–magnetic) anion can be modelled by *superexchange* and *semicovalence*.

Goodenough argues that if the cation (Mn) is located in an interstitial position of an octahedron spanned by anions (O), which is indeed the case in the perovskite structure, then the d–orbital of the cation will be split into a doubly degenerate e_g level and one triply degenerate t_{2g} level – see Fig. 2.3. The splitting is induced by the electrostatic field caused by the cation, and the amount of splitting, Δ, will depend strongly on its valence. Also, there will be a further split depending on the electron spin due to inter–atomic exchange interactions between the cation and anions [27]: In an anion–cation bond in which the anion has a full p–orbital overlapping an empty cation orbital, there will be two electrons of opposite spin in valence. In an ordinary homopolar bond these electrons have equal probability of being shared with the cation. But because there are exchange forces involved, and because the cation has a net magnetic moment in some direction, the situation changes in that the electron with spin parallel to the cation spin will have a greater probability

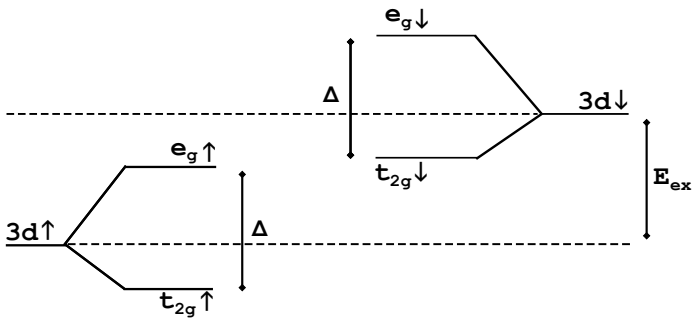

Figure 2.4: Splitting of the cation d–orbitals. Δ is caused by the self–induced electrostatic field and E_{ex} is caused by the exchange forces between the cation and anions [27].

of being shared. Also, the Pauli exclusion principle governs the spin state of the valence orbital in the anion [28]. This occasional addition of an electron to a neighboring cation corresponds to an even further split in the d–orbital of the cation, by an energy E_{ex}, see Fig. 2.4. The relation between the Δ and E_{ex} energies will determine whether the Mn atoms are in high or low spin states, which in turn determines the type of magnetic interaction between the two and hence also the total magnetic ordering of the structure, see Fig. 2.5 [27].

Kanamori [29] supplements Goodenough's picture by arguing that the symmetries of the orbitals are crucial. Overlapping orbitals of two atoms are considered orthogonal if they are invariant under collective spatial symmetry operations. It is stated that semicovalent bonds can only be formed between orbitals which are orthogonal.

The above arguments do, however, suppose that the Mn–O–Mn bond is linear, i.e. that the bonding angle is 180°. As seen in the two previous sections, this is not the case of the perovskite manganites; Octahedral tilting and JT distortion cause the bonds to be skewed to off–linear angles. Although Goodenough and Kanamori present valid results which are relevant as qualitative estimates, a more accurate model requires additional treatment. For instance, Kim et al. [30] use a microscopic Hamiltonian treatment and suggest that the nearest–neighbor interaction goes from slightly AFM to FM with increasing amount of JT distortion (i.e. decreasing bonding angle) and more AFM with increasing octahedral tilt angle. Kimura *et al.* [31], on their part, use a more phenomenological argument to conclude that the strongest superexchange interaction occurs where the geometry allows for the largest orbital overlap between neighboring Mn and O atoms, and arrive at the same qualitative result in regards to the magnetic ordering. These two works do, however, present quite contradicting results in other respects, something which will be discussed further in Sections 3.1 and 4.

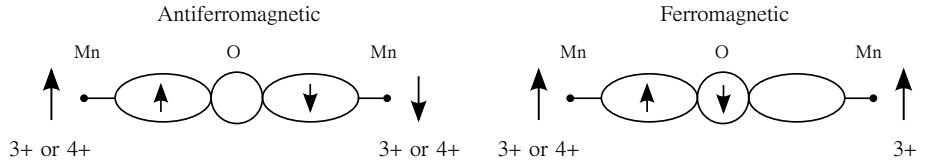

Figure 2.5: Schematic of the magnetic ordering in one Mn–O–Mn bond structure, resulting from the superexchange mechanism. The exchange depends strongly on the net ionic charge of the Mn atoms [28].

Chapter 3

Spin Modeling and Simulation

Most physical computer models are divisible into two parts, both of which are important for the results in their own right. Firstly, there needs to be a clear connection between the models and simulations and the real physics behind the experimental results that one may wish to target. To that end, a spin Hamiltonian in a lattice–geometry has been used here.

Secondly, the physical model must be implemented in such a way that the computational results reflect the real physics, and not just artefacts stemming from the mere fact that an artificial means has been used. In this thesis work, a flavor of the Monte Carlo method has been used to perform simulations within the spin Hamiltonian description.

3.1 The Heisenberg Model

The Heisenberg Model is a framework for describing interactions between magnetic atoms in a compound. It is very commonly used within the context of magnetic materials and spin modeling. In essence, it builds on formulating a microscopic lattice model Hamiltonian for the system. In its most rudimentary form, the Heisenberg Hamiltonian assumes pairwise interactions between closely situated spins – long–range interactions are usually neglected. A very common basic formulation is the following [16, 32]:

$$\mathcal{H} = \sum_{\langle i,j \rangle}^{\mathrm{NN}} J_{ij} \mathbf{S}_i \cdot \mathbf{S}_j + \sum_{\langle i,j \rangle}^{\mathrm{NNN}} J_{ij} \mathbf{S}_i \cdot \mathbf{S}_j \tag{3.1}$$

Here, the first sum is over nearest–neighbor (NN) spins and the second sum is over next–nearest–neighbor (NNN) spins. $\mathbf{S}_i$ is the vector of the spin at lattice site i. The factors J_{ij} are coupling constants reflecting the strengths of the interactions. The convention used in this work is that $J_{ij} < 0$ indicates a FM interaction and, conversely, $J_{ij} > 0$ indicates AFM.

One quickly realizes, however, that the Hamiltonian in Eq. (3.1) is not always enough to simulate more complex structures and phenomena. A fundamental challenge in working with Heisenberg physics is formulating a suitable Hamiltonian. In many cases, there is a need for a more detailed description. For instance, how does one take into account the dependence of the interactions on the positions of the O atoms in the perovskite structure?

As mentioned previously, it is the Mn atoms, with spin $S = 2$ (equivalent to a magnetic moment of $4\mu_B$, where μ_B is the Bohr magneton), which are magnetic – the other elements in manganese perovskites contribute indirectly. Thus, the Heisenberg Model would only take into account interactions between the manganese atoms, but attempts must be made to model the secondary effects stemming from interactions with the other elements in the structure.

Furthermore, it is seen from Section 2.1 that the differences between the expected magnetic phases are distinguishable in a two–dimensional geometry and hence it would be enough to simulate over one crystallographic *ab*–plane only. The different *ab*–planes are antiferromagnetically stacked in the manganese perovskites, and so certain ordering in one plane will have an equivalent in the other planes. The Hamiltonian used in this work is in spirit of Mochizuki [9]. In his work, a three–dimensional Hamiltonian is used which takes into account this antiferromagnetic spin–spin coupling in between planes. These Heisenberg exchanges along the *c*–axis are isotropic, whereas the NN–couplings in the *ab*–plane are modulated by the fact that magnetic interactions are screened by the intermediate oxygen atoms, and that the coupling strength depends on their positions. Oxygen deviations along the *c*–axis are, however, neglected in the works by Mochizuki, and the static screening is absorbed into the *c*–axis coupling. The fact that the JT effect is neglected along the *c*–axis further motivates that a two–dimensional Hamiltonian is sufficient. A drawback from using the 2D–lattice is that the anisotropies (single–ion and Dzyaloshinskii–Moriya anisotropies) will not be as elaborate as in the case of the 3D–model used by Mochizuki. For instance, the Dzyaloshinskii–Moriya interaction is neglected entirely in the present Hamiltonian so as to simplify calculations. It will, however, turn out to be an important term to consider (refer to Section 4.1). In this work, the total Hamiltonian has the following form:

$$\mathcal{H} = \mathcal{H}_{exc} + \mathcal{H}_{ani} + \mathcal{H}_{sl} + \mathcal{H}_{lat}, \tag{3.2}$$

where

$$\mathcal{H}_{exc} = J_{ab} \sum_i \left[\mathbf{S}_i \cdot \mathbf{S}_{i+\hat{\mathbf{x}}} + \mathbf{S}_i \cdot \mathbf{S}_{i+\hat{\mathbf{y}}}\right] + J_a \sum_i \mathbf{S}_i \cdot \mathbf{S}_{i+\hat{\mathbf{a}}} + J_b \sum_i \mathbf{S}_i \cdot \mathbf{S}_{i+\hat{\mathbf{b}}}, \tag{3.3}$$

$$\mathcal{H}_{ani} = A \sum_i \left(\mathbf{S}_i \cdot \hat{\mathbf{c}}\right)^2, \tag{3.4}$$

$$\mathcal{H}_{sl} = J_{sl} \sum_i \left[\delta_{i1} \mathbf{S}_i \cdot \mathbf{S}_{i+\hat{\mathbf{x}}} + \delta_{i2} \mathbf{S}_i \cdot \mathbf{S}_{i+\hat{\mathbf{y}}}\right], \tag{3.5}$$

$$\mathcal{H}_{lat} = K \sum_i \left[\delta_{i1}^2 + \delta_{i2}^2\right]. \tag{3.6}$$

Here, the sums run over all (manganese) atoms in one *ab*–plane of the lattice and the sub–index vectors are unit steps in the $\mathbf{x}, \mathbf{y}, \mathbf{a}$ and $\mathbf{b}$ directions. $\mathcal{H}_{exc}$ is the conventional Heisenberg exchange term, where J_{ab} is the NN interaction and J_a and J_b are NNN interactions. $\mathcal{H}_{ani}$ is an anisotropy term, making alignment along the out–of–plane *c*–axis less favorable. $\mathcal{H}_{sl}$ is a spin–lattice coupling term which takes into account the deviations of the oxygen atoms from their equilibrium positions so as to model octahedral tilting and the JT effect. The values δ_{i1}, δ_{i2} are (dimensionless) shifts in the $\hat{\mathbf{x}}$ and $\hat{\mathbf{y}}$ directions, respectively. They are scaled to assume values $-0.5 \leq \delta_i \leq 0.5$ depending on whether the bonding angle increases or decreases: Negative values indicate a smaller bonding angle and more ferromagnetic interactions and positive values indicate a more linear Mn–O–Mn bond, i.e. more AFM interactions. Finally, $\mathcal{H}_{lat}$ is an elastic term which favors the oxygen atoms being in their equilibrium positions, thus restoring the elastic force in the linear approximation. Figure 3.1 shows a schematic of the couplings. Table 3.1 summarizes the signs of the coupling constants in the Hamiltonian.

It is worth noting that this is not the only kind of Hamiltonian commonly used. There exist many works in which spin–lattice terms and single–ion anisotropies are not used, but rather one includes so–called *biquadratic couplings* in the model. These kinds of terms have been reported to also render good agreement with experimental data and first–principle calculations, and there is an ongoing debate about the validity of biquadratic additions as compared to a Hamiltonian on

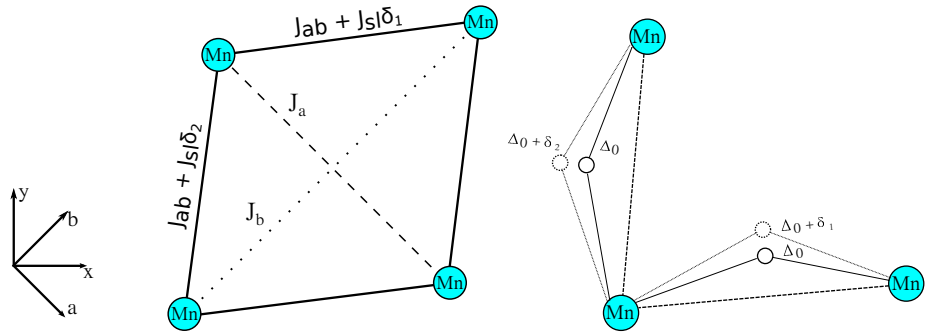

Figure 3.1: Schematic of the Heisenberg couplings in the Hamiltonian (3.2). White circles represent oxygen atoms and their shifts by δ_i from equilibrium.

the form (3.2), and concensus has yet to be reached. Refer to Section 4.1.5 for a more elaborate discussion.

3.1.1 Strain Modeling

It has been shown that the Néel temperature, i.e. the transition temperature from PM to AFM, of tetragonal perovskites changes under strain [33]. But how does one model this? Once the Heisenberg parameters in Table 3.1 have been fit to match the relaxed phase diagram sought after, it remains to systematically account for the strains in the lattice by altering the Hamiltonian in a suitable way. This requires some insight into how the manganese perovskite structure deforms under the influence of strain.

Intuitively, and referring to, for instance, Fig. 2.2, it is the lattice parameters a and b that change under the influence of ab–plane strain. Indeed, this is what has been reported [15, 34]. In the context of the Hamiltonian (3.2), this would correspond to altering of the exchange couplings J_{ij} by different amounts. It has been shown that the NN couplings are are rather sensitive to strain in the ab–plane, while the NNN couplings show no significant change in comparison [34]. This would correspond to scaling J_{ab} and J_{sl} in the Hamiltonian above.

Table 3.1: Summary of exchange couplings in the Hamiltonian (3.2).

Description	Abbreviation	Sign
NN	J_{ab}	$-$
NNN	J_a	$-$
NNN	J_b	$+$
Anisotropy	A	$+$
Spin–lattice	J_{sl}	$+$
Elasticity	K	$+$

When the in–plane lattice parameters change, the Mn–O–Mn bonding angles will be affected as well. Previous results are, however, not consistent in describing *how* they are affected. Experiments performed using X–ray diffraction on epitaxially strained thin–films have shown that the thinner the films (i.e. the higher the strain), the larger the in–plane bonding angle [15]. That is, thin–films with higher ab–plane strain experience a more antiferromagnetic Mn–O–Mn interaction. On the other hand, first–principle calculations have shown that the in–plane Mn–O–Mn bonds do not

change notably under neither compressive nor tensile *ab*–plane strain. Rather, it is the inter–plane Mn–O–Mn angles that are suggested to change – and quite drastically, too [34]. In the two–dimensional model chosen for this work, there is no way of accounting for the intra–plane interactions, and hence attempts are made to follow the results reported in [15]. In the context of the Heisenberg Hamiltonian above, an altered Mn–O–Mn bonding angle corresponds to a shift of Δ_0 in Fig 3.1. Now, since the NN coupling J_{ab} is set to be FM, it follows that an increased bonding angle (i.e. a decreased Δ_0) corresponds to a more AFM J_{sl} coupling. That is, the products $J_{sl}\delta_{i,i+\hat{x}}$ must increase with the bonding angle.

3.2 Monte Carlo Simulations

When investigating properties of a spin system at finite temperatures, the goal is usually to deduce expectation values of some physical observables and study how they change in a certain temperature range. A suitable environment is the canonical ensemble, in which Boltzmann statistics are applicable [16]. A proper thermal expectation value of the observable M in this context would be $\langle M\rangle = \frac{1}{Z}\sum_i M_i p_i \exp(-\beta E_i)$, where i runs over all possible states M_i with probabilities p_i. Here, $\beta = 1/k_b T$ is the inverse thermal energy, E_i is the energy of the state and Z is the partition function [32]. But since there may be up to an infinite number of possible states in the system, this approach is not feasible in the context of computer simulations. Instead, one can approximate $\langle M\rangle$ by means of *importance sampling*, in which the expectation value over a chain of events is taken to be the "time average" over the states M_i that the system assumes in the chain:

$$\langle M\rangle = \frac{1}{N}\sum_{i=1}^{N} M_i. \tag{3.7}$$

This much simpler sum runs over the N states assumed by the system over the chain. Here, the Boltzmann factor and the impractical partition sum over all possible states have been canceled out. The connection to the canonical ensemble and Boltzmann statistics now appear only in how one choses the allowed states M_i [13]. Eq. (3.7) is fundamental to Monte Carlo (MC) simulations. It remains now to introduce a scheme for generating the set of allowed states in this sum. At the heart of doing this are *Markov processes*: Given a state M_i, one randomly generates a new state M_j and accepts the transition to the new state with a probability $P(M_i \to M_j)$. If accepted, the system is then said to be in state M_j, otherwise it remains in M_i. If one performs these *trial moves* repeatedly, the series of transitions is called a *Markov chain*, and it is over this chain that one computes the thermal average (3.7) [13]. In the context of our two–dimensional spin–lattice, the states M_i and M_j are different configurations of spin directions, and the transition probability $P(M_i \to M_j)$ is governed by the Boltzmann distribution.

3.2.1 The Metropolis Algorithm

One of the most common simulation schemes in statistical physics (and in a variety of other fields as well) is the *Metropolis Algorithm*, proposed by Metropolis *et al.* in 1953 [35]. In short, it builds upon studying the energy difference between the current state M_i and a randomly generated new state M_j and favor accepting states M_j which have lower energy than M_i. But in order for the Markov chain to be consistent with Boltzmann statistics, there must also be a finite probability for M_j to be accepted even if it has higher energy. Thus, the Metropolis probability is expressed as follows [13]:

$$P(M_i \to M_j) = \begin{cases} e^{-\beta\Delta E}, & \Delta E > 0 \\ 1, & \text{otherwise} \end{cases}, \tag{3.8}$$

where $\Delta E = E_{M_j} - E_{M_i}$. In a conventional Metropolis scheme applied to a spin system, and given a set of temperatures, one would begin by fixing the temperature in either end of the range. Then, one would perform N trial moves in a Markov chain and accept or reject them according to Eq. (3.8). After forming the thermal averages of interest (such as magnetization, energy, etc.), a new temperature is chosen and the procedure is repeated. When all temperatures have been visited, one has a sense of how the thermal averages change within the range. Naturally, the number of trial moves per sample, and the number of samples, N, strongly influences the accuracy. Also, the number of temperatures visited within the range plays an important role.

3.2.2 Replica Exchange and Parallel Tempering

The method described above does, however, suffer from a few drawbacks. If the system is complex enough, there may exist several energy minima in the low–temperature regime. These minima are separated by energy barriers, and it can be a challenge to overcome them using the standard Metropolis Monte Carlo method [36]. This is because, at low temperatures, acceptance rates are lower due to the low thermal energy in the system, and therefore one would have to perform many trial moves before potentially escaping a local minimum in the free energy landscape. As mentioned previously in Section 2.1.1, this is a real issue in manganese perovskites, because there is a range of R elements with atomic radii such that there are several possible phases at low temperatures – the E–type may coexist with the spin spiral [12] and even the different kinds of spin spirals may coexist with each other in certain cases [5]. Also, when modeling the perovskite manganites in the Heisenberg framework, different combinations of values of the coupling constants in Table 3.1 may give rise to degenerate phases [9], which are difficult to handle using the conventional Metropolis method.

One way of overcoming these issues is by using the *parallel tempering* (PT) or *replica exchange* algorithm. It builds upon creating a number of replicas of the spin system and place each of them at a different temperature in the range of interest. One then performs a number of conventional Metropolis trial moves so as to equilibrate each system at its given temperature. The main idea is then that there is a finite Boltzmann probability for a temperature exchange between each pair of replicas R_i and R_j according to [36]

$$P(R_i \longleftrightarrow R_j) = \begin{cases} e^{-\Delta_R}, & \Delta_R > 0 \\ 1, & \text{otherwise} \end{cases}, \tag{3.9}$$

where

$$\Delta_R = (\beta_j - \beta_i)(E_{R_i} - E_{R_j}). \tag{3.10}$$

Every once in a while, a trial move is made according to Eq. (3.9). If it is accepted, then the replicas are interchanged and the procedure is repeated. In order for the acceptance rates to remain relatively high, one may choose to only perform trial moves between "neighboring" replicas in the temperature range [36], but there are cases for which one may wish to sacrifice a high acceptance rate in exchange for, for instance, a more efficient computer implementation and perform trial moves for replicas that might not be neighbors [37].

3.3 Simulation Methodology

The spins of the manganese atoms in the structure were represented by classical vectors of fixed length and position, but free to rotate in any of the three dimensions. In this model, there are thus two free spatial parameters, namely the polar and azimuthal angles in Euclidian space. Also, since

all manganese atoms are connected to each other via an oxygen atom, the oxygen deviations $\delta_i^{x,y}$ from equilibrium are also free parameters so as to model the lattice distortions (refer to Sec. 2.3 and Fig. 3.1).

Spins were sampled for the MC sweeps by randomly chosing a c–axis component, S_{ci}, and a polar angle, θ_i, and then constructing the spin according to [9]

$$\mathbf{S}_i = \Big(\sqrt{S_i^2 - S_{ci}^2}\cos\theta_i, \sqrt{S_i^2 - S_{ci}^2}\sin\theta_i, S_{ci}\Big). \tag{3.11}$$

Oxygen deviations $\delta_i^{x,y}$ in the x and y directions were sampled such that $-0.5 < \delta_i^{x,y} < 0.5$ [9].

Depending on the order parameters used to describe a certain kind of ordering, magnetic phase transitions can be detected in several different ways. Two common observables in this context is the heat capacity, C_v, and the magnetic susceptibility, χ. They can be defined in a statistical manner by

$$C_v = \frac{\beta}{T}\big(\langle E^2\rangle - \langle E\rangle^2\big), \tag{3.12}$$

$$\chi = \beta\big(\langle m^2\rangle - \langle m\rangle^2\big). \tag{3.13}$$

In addition to studying the order parameter(s), a phase transition can be identified by divergent C_v and χ at the transition temperature [13].

Different types of magnetic ordering have different call–signs by which they can be identified. For instance, a completely ferromagnetic configuration will have a finite magnetization, whereas a fully antiferromagnetic structure will have zero net magnetization. When it comes to spin states that cannot be described as either or, other means are necessary. Important tools are the two main types of *correlation functions* [13]:

- Real–space spatial (spin) correlation functions in an equilibrium system measure the range of the ordering and can be defined as

$$\bar{S}(\mathbf{r}) = \frac{1}{N}\sum_{i,j}\left[\langle \mathbf{S}_i \cdot \mathbf{S}_j\rangle - m^2\right], \tag{3.14}$$

  where N is the number of atoms in the system and $\mathbf{r} = \mathbf{r}_i - \mathbf{r}_j$ is the distance between spins $\mathbf{S}_i$ and $\mathbf{S}_j$ and m is the average magnetization in the system.

- Reciprocal–space (spin) correlation functions measure the ordering in the frequency domain when moving along some axis, α, and can be defined as

$$\begin{aligned}\hat{S}_\alpha(\mathbf{k}) &= \frac{1}{N}\sum_{\mathbf{r}} e^{i\mathbf{k}\cdot\mathbf{r}}\bar{S}_\alpha(\mathbf{r}) \\ &= \frac{1}{N}\left\langle \sum_{\mathbf{r}_i} e^{-i\mathbf{k}\cdot\mathbf{r}_i}(S_{i\alpha} - m)\sum_{\mathbf{r}_j} e^{i\mathbf{k}\cdot\mathbf{r}_j}(S_{j\alpha} - m)\right\rangle.\end{aligned} \tag{3.15}$$

  This is equivalent to the Fourier transform of the observable. Here, $\bar{S}_\alpha$ denotes the correlation of the spin component in the α direction in real space.

The most important magnetic phases of those described in Section 2.1.1 are the E–type AFM phase the incommensurate spin spirals in the *ab*– and *bc*–planes, and the incommensurate sinusoidal phase. They can be identified as follows (see Table 3.2) [9]:

- In the E–type phase, the b–components of the spins are modulated by a wave vector of around $k_b \sim 0.5\pi$. There are suggestions saying that it is commensurate, with k_b exactly equal to 0.5π [9], but other sources say that it is incommensurate, with $k_b \approx 0.49\pi$ [2]. In any case, Eq. (3.15) is used to calculate the frequency response of the b–axis spin components. Also, it has been suggested that the reciprocal–space correlation function for the oxygen deviations δ_i has sharp peaks for $\mathbf{k} = (\pm\pi, \pm\pi, 0)$ [9]. It is defined as follows:

$$\hat{\delta}_{\gamma,\gamma'}(\mathbf{k}) = \frac{1}{N^2} \sum_{i,j} \langle \delta_{i,i+\gamma} \delta_{j,j+\gamma'} \rangle e^{i\mathbf{k}\cdot(\mathbf{r}_i - \mathbf{r}_j)}, \tag{3.16}$$

  where $(\gamma, \gamma') = (x,x), (y,y)$ and (x,y). i and j each runs once over all spins in the system.

- The incommensurate ab–plane spiral and the sinusoidal collinear phases are shown to have sharp peaks in $\hat{S}_b$ (Eq. (3.15)) for wave vector $\mathbf{k} \approx (0.46\pi, 0.46\pi, \pi)$ [38], although early experiments suggested that there is no lock–in to any fixed value within this phase region [5]. Similarly for the bc–plane spiral, the $\hat{S}_c$ correlation function has a sharp peak for the same value of $\mathbf{k}$ [38]. The spiral and sinusoidal collinear phases are told apart by constructing the *spin helicity* correlation function:

$$\hat{H}^b_\alpha(\mathbf{k}) = \frac{1}{N^2} \sum_{i,j} \langle h^b_{i\alpha} h^b_{j\alpha} \rangle e^{i\mathbf{k}\cdot(\mathbf{r}_i - \mathbf{r}_j)}, \tag{3.17}$$

  where $\mathbf{h}^b_{i\alpha} = \frac{1}{S^2}(\mathbf{S}_i \times \mathbf{S}_{i+b})_\alpha$ are the local spin helicity α–components. In the sinusoidal region, $\hat{H}^b_\alpha$ is practically zero everywhere, whereas, for the ab and bc–spirals, there are peaks for $|\mathbf{k}| = 0$ in $\hat{H}^b_c$ and $\hat{H}^b_a$, respectively [38].

Table 3.2: Summary of the characteristics of different phases.

Phase	$\hat{S}_b$	$\hat{S}_a$	$\hat{S}_c$	$\hat{H}^b_a$	$\hat{H}^b_c$	$\hat{\delta}_{\gamma,\gamma'}$
bc–spiral	$\neq 0$	$= 0$	$\neq 0$	$\neq 0$	$= 0$	N.A.
ab–spiral	$\neq 0$	$\neq 0$	$= 0$	$= 0$	$\neq 0$	N.A.
E–type	$\neq 0$	$\neq 0$	$= 0$	$= 0$	$\neq 0$	$\neq 0$
Sinusoidal	$\neq 0$	$= 0$	$= 0$	$= 0$	$= 0$	N.A.

3.3.1 Computer Implementation

In this work, a Monte Carlo program was written in its entirety. A square ($L \times L$) lattice was used, with periodic boundary conditions (PBCs). The Metropolis algorithm was implemented according to the above. Also, parallel tempering was used so as to improve statistics and to overcome potential minimum–energy traps. The latter was implemented using the *Message Passing Interface* (MPI), in which each replica of the system is run as an independent thread. When replica exchange trial moves are performed, messages containing the total energy and temperature of the replica are sent in–between threads. An accepted trial move is equivalent to interchanging the temperature values of the participating replicas. In the implementation used, all processes perform Heisenberg Monte Carlo calculations, but one of the threads is thought of as *master* in that it also performs the PT trial moves between all threads and distributes messages amongst them. A *decentralized* PT algorithm has been proposed in which all threads perform these exchanges [37]. An advantage of this method is that the PT trial moves are performed "locally" by the two replicas involved. This

makes for a faster program since there is no longer only one thread having to serially pass messages to all the others. This decentralized PT algorithm is, however, not explored any further in this work.

Computer code was written in the C language and simulations were run using bash scripts. Random numbers were generated using the GNU Scientific Library[1]. The MPI was implemented using the open–source Open MPI library[2].

Typically, in order to observe the expected phenomena described in Section 2.1, there is a need for quite large lattices (up to some 100×100 atoms). Also, a fine temperature mesh requires many replicas (some 100) to be run in parallel. These needs are difficult to meet with a regular computer, and therefore some of the simulations have been run on the Triolith cluster at the National Supercomputer Centre (NSC) at Linköping University. Using this resource, each replica could be dedicated one processor of its own and much larger computations could be performed.

[1] https://www.gnu.org/software/gsl/
[2] http://www.open-mpi.org/

Chapter 4

Simulation Results and Discussion

Simulations were performed in two steps. Firstly, attempts were made to tune the model to reproduce results obtained by others for the unstrained case so as to validate the written MC program. Then, simulations were performed using a model of the strained case. Results from these two scenarios are presented and discussed below.

4.1 Unstrained Case

Figure 4.1 shows a schematic of the predicted phase diagram for different R elements [5, 38]. In the model Hamiltonian (3.2), it is the NNN coupling J_b which reflects the differences between the choices of R; Large R atoms are modeled with small values of J_b, and vice versa [9].

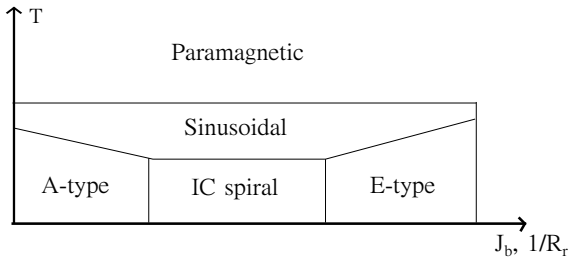

Figure 4.1: Schematic of the magnetic phase diagram as a function of the inverse size of the R element or, equivalently, the value of the parameter J_b [5, 9].

It is seen in Fig. 4.1 that the low–temperature phase becomes increasingly antiferromagnetic in the ab–plane for smaller R atoms. That is, the relatively strongly ferroelectric E–type phase appears for R = Ho-Lu in the lanthanide series. However, the true characteristics of this phase are not entirely clear – there are reports of a range of different results when it comes to the E–type phase. The ideal E–type configuration, as seen in Fig. 2.1(c), is commensurate with $k_b = 0.5\pi$ [9]. However, other results point towards that the real E–type phase experiences a slight in–plane modulation, with wave vector $k_b \approx 0.48\pi$ [2, 30]. The modulation is attributed to a single–ion anisotropy and to the Dzyaloshinskii–Moriya (DM) interaction and arguments have been put forward that this "incommensurate E–type" ordering is a question of a coexistence between the IC spiral in the bc–plane and the purely E–type phase [9].

Table 4.1: Simulation parameters used together with Eq. (3.2) in the simulations of the unstrained system. The J_b parameter was varied in the simulations so as to model the different R atom radii. All values are in units of meV.

J_a	J_b	J_{ab}	J_{sl}	A	K
-1.0	$1.0 \rightarrow 4.5$	-0.8	2.5	0.1	500

Simulations were performed using Eq. (3.2) and a 100×100 lattice. The coupling parameters J_{ab}, J_{sl}, A and K where gathered either from experiments or theoretical estimates by others, and compiled by Mochizuki [9]. The value of the ferromagnetic NN coupling J_a was set higher than in [9] because it yielded better agreement with previous results in the present 2D–lattice. A summary of the parameters used are presented in Table 4.1. Replica exchange attempts were made every 200 MC sweeps, where each sweep consisted of $L \times L$ trial moves (that is, 10^4 in this case). $3000 \times p$ replica exchange attempts were performed, where $p = 96$ is the number of replicas used over the temperature range.

4.1.1 Incommensurate Spiral Phases

Figure 4.2 shows the phase diagram for the system when varying the J_b parameter. It is seen that the phase boundaries in the temperature domain agree rather well with what has been previously reported for lower values of J_b. Low–temperature phases were identified according to the rules of thumb in Table 3.2. There is, however, no clear distinction in the results between the two different types of IC spirals. Instead, there are simultaneously peaks in the $\hat{S}_a$ and $\hat{S}_b$ data for the low–temperature region, something which would signify a coexistence of the two kinds of spirals or, rather, a kind of incommensurate pseudo–state which is of neither ab or bc–spiral kind. The regions in Fig. 4.2 marked as IC spirals are done so based on which of $\hat{S}_a$ and $\hat{S}_b$ is dominating, but in no case is any flavor of spiral phase particularly well–distinguishable from the other here.

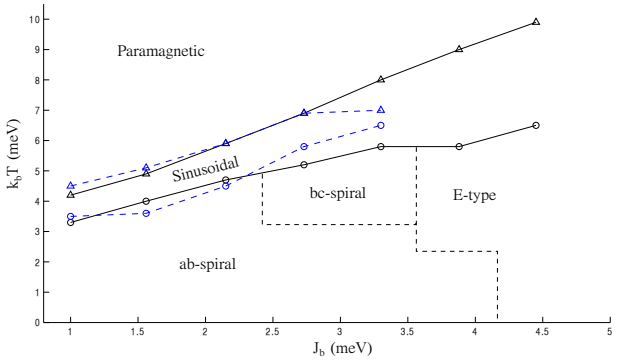

Figure 4.2: Approximate phase diagram obtained from simulations of the unstrained case (black lines). Blue lines are previously presented theoretical results [9]. Black dashed lines are approximate phase evolutions using the present model.

Table 4.2: Approximate phase evolutions as a function of the parameter J_b – comparison with previous results.

Transition	J_b (meV)	
	This work	[9]
$ab \rightarrow bc$	~ 2.5	~ 0.8
Spiral$\rightarrow$E–type	~ 3.7	~ 2.0

To understand the inability of the model Hamiltonian (3.2) to distinguish between the two kinds of spiral phases, one has to study their reported origins. One common effect to take into account in a Heisenberg Hamiltonian describing manganese perovskites is the Dzyaloshinskii–Moriya

interaction. It has terms on the form $\mathbf{d}_{ij}^{\alpha} \cdot (\mathbf{S}_i \times \mathbf{S}_j)$ which favors canting of otherwise parallel spins. The vectors $\mathbf{d}_{ij}^{\alpha}$, where $\alpha = \{x, y, z\}$, reflect the bond geometries of the structure and can be determined via experiments or first–principle calculations [5, 38]. In the $R\mathrm{MnO_3}$ structure, shifts of the in–plane oxygen atoms due to JT distortion and octahedral tilting will alter the c–components of the $\mathbf{d}_{ij}^{\alpha}$ vectors. This favors an ab–plane cycloid since the in–plane spins strongly couple with these c–components. It has been shown in [38], however, that the energy gain of the ab–phase due to the DM interaction reduces with increasing oxygen shifts (and hence also with decreasing R element size and increasing J_b). Thus, there becomes room for another phase with lower energy – in this case the bc–phase, whose energy gain is independent of the value of J_b. The bc–plane phase is really a modulation of the angles ϕ_c between inter–plane neighbor spins, which are equal to $\phi_c = \pi$ in the absence of any DM terms due to strongly antiferromagnetic inter–plane interactions in the models used in [9, 38]. But when the DM term sets in, oxygen shifts will affect these interactions via alterations of the ϕ_c angles, and the bc–cycloid can be formed.

In regards to the above, the model Hamiltonian used in the present work is insufficient. It is two–dimensional and fails by construction to reflect the inter–plane antiferromagnetic behavior, from which the bc–spiral is assumed to appear. There is only one term taking into account the coupling to the c–axis, namely the single–ion anisotropy $\mathcal{H}_{ani}$ in the Hamiltonian. Now, considering a small change in the angle ϕ_c' between a spin and the c–axis by $\Delta\phi_c'$, we have via Eq. (3.4) that

$$\begin{aligned} \Delta E_{ani}/N &= AS^2 |\cos^2(\phi_c' + \Delta\phi_c') - \cos^2\phi_c'| \\ &= \frac{1}{2} AS^2 |\cos(2\phi_c' + 2\Delta\phi_c') - \cos 2\phi_c'| \approx \frac{1}{2} AS^2 |\sin(2\phi_c')\Delta\phi_c'|. \end{aligned} \tag{4.1}$$

It is seen here that there is always an energy cost for spins to direct themselves out of the ab–plane – the c–axis is a *hard axis* for the magnetization and the system has a steady minimum for $\phi_c' = \pi/2$. Were the DM term present, there would be a competition between it and the anisotropy term (3.4), leading to an energy gain for canting in the c–direction when increasing J_b [38]. But since Eq. (3.2) includes no DM interaction, the spins will have a hard time shifting from their equilibrium position and move in a spiral fashion and this is a reason for the absence of a bc–spiral in the phase diagram in Fig. 4.2.

The ab–cycloid appears due to the superexchange term $\mathcal{H}_{sl}$ in the present Hamiltonian. It will, however, rotate uniformly in all directions in the ab–plane – contrary to the expected b–directed cycloid – because the in–plane angle ϕ_{ab} between two neighboring spins only depends on the ratio between the NN and NNN couplings and there would practically always be an energy gain of having this phase. If the DM interaction were present, however, the energy gain would decrease with increasing structural distortion (increasing J_b) until the bc–spiral became energetically favorable and the phase evolution took place [9, 38]. Thus, to summarize, the two–dimensional lattice model and the absence of the DM interaction in the Hamiltonian are what hinder there being a distinction between the two possible spin spirals in $R\mathrm{MnO_3}$.

4.1.2 E–type Ordering

With increasing J_b comes an onset of the periodic modulation of the oxygen shifts δ_i in the Mn–O–Mn bonds and the E–type phase is formed. It has been shown that the crucial interactions in the Hamiltonian for forming the E–type phase are the Heisenberg exchanges J_{ab}, J_a and J_b and the superexchange term J_{sl} [9]. Figure 4.3 shows the peak wave vector evolution for $\hat{S}_b$. It is seen that the modulation moves towards being commensurate with 0.5π as J_b is increased. The E–type phase is identified as having set in when peaks appear for $\hat{\delta}_{yy}$ in the low–temperature region as seen in the inset of Figure 4.3. But using the parameters in Table 4.1, the fully commensurate

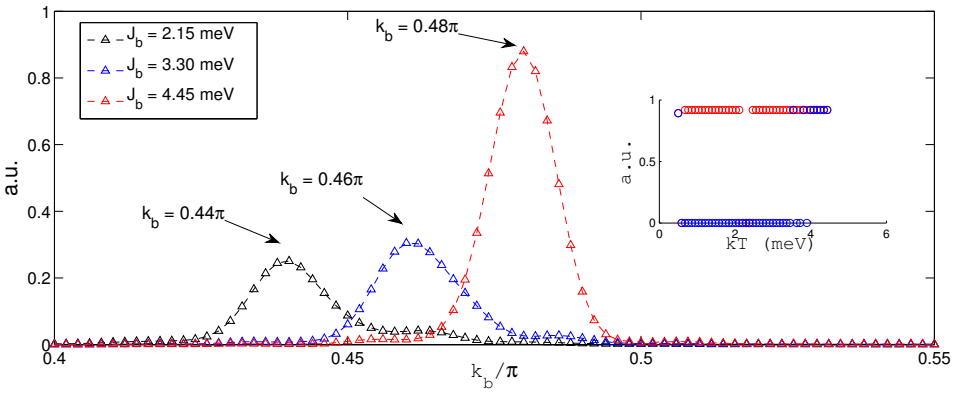

Figure 4.3: Peak values of the $\hat{S}_b$ correlation function (3.15) at $k_bT = 3.4$ meV. The black, blue and red plots are for $J_b = 2.15, 3.3$ and 4.45 meV, respectively. All other parameters in Eq. (3.2) were set according to Table 4.1. The first two are identified as IC–spirals and the latter is an (incommensurate) E–type phase. Inset: Peak values of $\hat{\delta}_{yy}$ as defined in Eq. (3.16) for wave vector $k_b = \pi$. It is seen that only the high–J_b phase has non–zero correlation for low temperatures, thus signifying an E–type phase.

configuration expected for a theoretical E–type phase does not seem to form for any reasonable value of J_b. Rather, the E–type phase has a strong peak for $k_b = 0.48\pi$, something which is described by some as a coexistence between the E–type phase and an IC–spiral [9] and by others as a coexistence with the sinusoidal collinear phase [2]. Indeed, it is seen that it is the single–ion anisotropy (and possibly also the DM term) which obstructs the full commensurability in the E–type region. Figure 4.4 shows a comparison between two E–type phases, one of which is a result of the full Hamiltonian (3.2) and the other of which does not include $\mathcal{H}_{ani}$ or $\mathcal{H}_{lat}$. Clearly, one is commensurate while the other is not, thus proving the importance of considering such extra terms in the Hamiltonian. The question remains, however, whether the pure commensurate E–type phase is really feasible.

Experiments reveal that different samples have different E–like ordering; $LuMnO_3$ thin films have been shown to have incommensurate E–type ordering [2] while a commensurate E–phase has been identified in bulk $LuMnO_3$ samples [39], and so one may conclude that anisotropies play more important roles and that canting along the c–axis is more prominent in more 2D–like samples.

4.1.3 Sinusoidal Collinear Phase

The sinusoidal collinear phase appearing above the low–temperature phases throughout the sweep in J_b–space in Fig. 4.2 increases more than expected in comparison to the results presented in [9]. Again, this is attributed to the fact that there exists no DM term in the Hamiltonian, thus making the single–ion anisotropies dominate in the coupling to the c–axis. It has been demonstrated that an increasing amount of single–ion anisotropy increases the temperature range for which the sinusoidal collinear phase is stabilized [38].

4.1.4 Low–Temperature Phase Evolutions in J_b–Space

Looking at Fig 4.2 and Table 4.2, there is quite a discrepancy in where the phase evolutions between the different low–temperature phases occur when gradually increasing the J_b parameter; Results in this work severely overestimate the J_b values for which the evolutions take place as compared

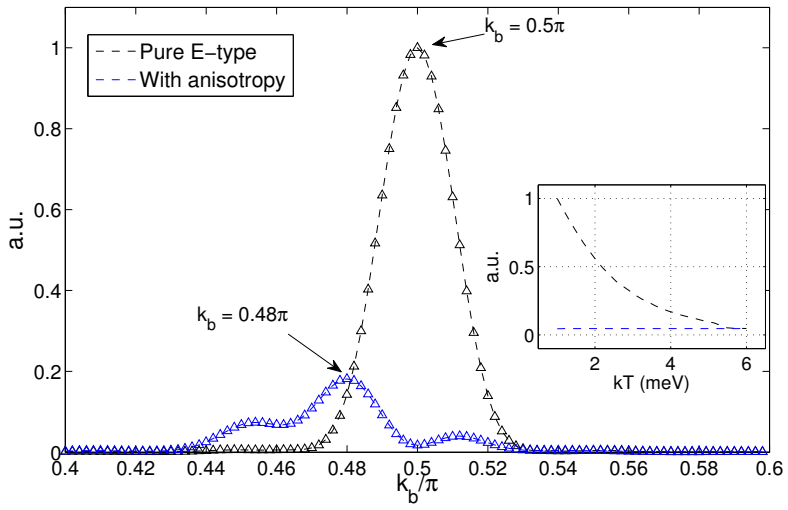

Figure 4.4: Peak values of the $\hat{S}_b$ correlation function for simulations run with (black) and without (blue) single–ion anisotropies and elastic terms in the Hamiltonian. In both cases, $J_b = 4.45$ meV and $k_bT = 3.4$ meV. Without $\mathcal{H}_{ani}$ and $\mathcal{H}_{lat}$, it is seen that the system is able to become fully commensurate, whereas it locks into $k_b = 0.48\pi$ in the presence of these terms. Inset: Peak values for $\hat{\delta}_{yy}$ in the respective cases. It is seen that, while both phases have non–zero values (and hence are E–type), the commensurate phase has much stronger correlation in the low–temperature regime.

with previous results in [9]. This can be attributed to the absence of DM interactions which, in combination with the single–ion anisotropy term, establishes the spin–cycloids (see discussion above): Previous results show phase evolutions from a *bc*–spiral to the E–type, which are clearly distinctive from each other in that the *bc*–spiral is an out–of–plane modulation and the E–phase is an in–plane antiferromagnetic ordering. Mochizuki [9] reports a coexistence of these two phases for a range of J_b values – that is, an E–phase with canting along the *c*–axis. Now, since the present model only has in–plane spin–spin couplings and fails to reproduce a clear *bc*–spiral, the evolution takes place between the *ab*–spiral and the E–type phases. Given a set of parameters such that the system is in proximity to the point of transition between these two phases, the energy difference per spin is (by Eq. (3.2) and the geometries of the phases)

$$\begin{aligned}\Delta E_{ab\to E} &= E_E/N - E_{ab}/N \\ &= S^2\big[J_a - J_b\big] - S^2\left[2J_{ab}\cos\frac{\phi_b}{2} + J_a + J_b\cos\phi_b + J_{sl}\cos\frac{\phi_b}{2}\underbrace{(\bar{\delta}_x^{ab} + \bar{\delta}_y^{ab})}_{<0}\right] \\ &= S^2\left[2|J_{ab}|\cos\frac{\phi_b}{2} + J_{sl}\cos\frac{\phi_b}{2}|\bar{\delta}_x^{ab} + \bar{\delta}_y^{ab}| - J_b(1+\cos\phi_b)\right], \end{aligned} \tag{4.2}$$

where $\bar{\delta}_i^X$ is the average oxygen shift in the i direction for phase X and ϕ_b is the incommensurate modulation angle in the b–direction for the *ab*–spiral (which is shown above to be $\phi_b = 0.46\pi$). By symmetry, it can be assumed that the average oxygen shift $\bar{\delta}_i^E$, $i = x, y$, is isotropic, thus making the spin–lattice terms cancel in E_E. (Assuming also that the $\bar{\delta}_i^X$ are small, the elastic terms from Eq. (3.6) cancel as well.) The relation $\bar{\delta}_x^{ab} + \bar{\delta}_y^{ab} < 0$ was established through the

MC simulations. Now, since the first two terms are positive and the third is negative, there is a competition between them, creating an energy gain for the E–type system only when increasing J_b by large enough amounts. Thus, theoretically, there will eventually be a phase evolution from the ab–phase to the E–type phase and it is the relative values of J_{ab}, J_{sl} and J_b which determine the point of evolution. Interestingly, the ferromagnetic J_a coupling has no part in determining the phase evolution. Also, since $\bar{\delta}_i^{ab}$ are small, one may neglect the J_{sl} term in Eq. (4.2), and so the stabilization of the E–phase can be said to depend only on the ratio between J_{ab} and J_b. Using $S = 2$ and parameter values in Table 4.1, we see that $J_b > 4.3$ meV for the E–type phase to be established with the present Hamiltonian, thus explaining the difference as compared to the results in [9].

4.1.5 Biquadratic Couplings

The present Hamiltonian (3.2) only takes into account exchanges up to bilinear order. Mochizuki reports that Equations (3.3) and (3.5) are enough to establish the pure E–type phase [9]. But there are essentially two main doctrines by which current researchers choose to describe manganese perovskites, one of which follows Kimura [6] and Mochizuki [9, 12, 38] and is used in this work. The other, described for instance in [40, 41], use Hamiltonians in which there are no single–ion anisotropies, DM interactions or spin–lattice couplings. Instead, arguments are put forward that quartic couplings are the ones to establish the E–type phase. This type of coupling term is suggested by Hayden *et al.* [41] to be biquadratic and have the form

$$\mathcal{H}_{bq} = \kappa_{bq} \sum_{ij} (\mathbf{S}_i \cdot \mathbf{S}_j)^2, \tag{4.3}$$

where the sum is performed for NN spins. Fedorova *et al.* suggest instead that, in addition to the biquadratic exchange, a quadratic four–spin ring exchange is also important [40]. It has the form

$$\mathcal{H}_{4q} = \kappa_{4q} \sum_{ijkl} \big[(\mathbf{S}_i \cdot \mathbf{S}_j)(\mathbf{S}_k \cdot \mathbf{S}_l) + (\mathbf{S}_i \cdot \mathbf{S}_l)(\mathbf{S}_k \cdot \mathbf{S}_j) - (\mathbf{S}_i \cdot \mathbf{S}_k)(\mathbf{S}_j \cdot \mathbf{S}_l) \big]. \tag{4.4}$$

Here, the sum is performed for NN spins forming a ring–like, four–site plaquette. Both above forms of quartic couplings are claimed to describe better the origins of the E–type ordering. In fact, Kimura [6] is refuted almost entirely in a comment by Kaplan [42] in which it is shown that the pure exchange Heisenberg Hamiltonian (3.3) fails to stabilize the E–type phase. The model of Kimura *et al.* has since been extended by Mochizuki [9] to include terms on the form (3.5), directly taking into account the structural distortions of the perovskite structure which render the NN couplings anisotropic, and thus making it possible for the E–type phase to form. In fact, it is stated there that Eq. (3.5) is crucial for lifting the degeneracy in the otherwise frustrated configuration, something which is not taken into consideration in, for instance, the paper by Fedorova in which the pure Heisenberg description is deemed insufficient [40]. In this paper, it is shown via first–principle calculations that the biquadratic couplings can be comparable in size to the bilinear couplings in orthorombic perovskite manganites with small R–atom radii. It is also demonstrated that the pure Heisenberg Hamiltonian (3.3) applied to $TbMnO_3$ renders energies which do not agree well with those calculated from density–functional theory (DFT), and that the addition of a biquadratic term greatly improves the results. Again, it should be stressed that comparisons are made with a Hamiltonian not including the $\mathcal{H}_{sl}$ term, the addition of which may be of interest for future similar studies.

Hayden *et al.* [41] make the claim that Eq. (4.3) is an important addition to the pure Heisenberg Hamiltonian in order to establish the E–type phase. It can be shown, however, that Eq. (4.3)

is equivalent to Eq. (3.5) by a simple argument: Consider a Hamiltonian which includes both spin–spin exchanges and phonon terms:

$$\tilde{\mathcal{H}} = J_{ij} \sum_{ij} \mathbf{S}_i \cdot \mathbf{S}_j + u\tilde{J}_{sl} \sum_{ij} \mathbf{S}_i \cdot \mathbf{S}_j + k\frac{u^2}{2} + \frac{p^2}{2m}, \tag{4.5}$$

where u is a harmonic oscillator variable and the last term is an ion momentum term. By arguing that u has a much slower time scale than do the spin interactions, the *adiabatic approximation* is valid. It states that, given a time interval $[0, T]$ in which the time scale argument above holds, a system which is in an eigenstate of $\tilde{\mathcal{H}}(u)$ is assumed to remain so throughout the time interval in the adiabatic approximation [43]. Thus, we have that $\frac{\partial \tilde{\mathcal{H}}}{\partial u} \approx 0$ in Eq. (4.5) and one can define a mean–field free energy, $E(u)$, according to

$$E(u) = J_{ij} \langle S_i S_j \rangle + \tilde{J}_{sl} \langle S_i S_j \rangle u + k\frac{u^2}{2}. \tag{4.6}$$

Minimizing with respect to u and reinserting into the expression then gives the following:

$$E(u) = J_{ij} \langle S_i S_j \rangle - \frac{\tilde{J}_{sl}^2}{2k} \langle S_i S_j \rangle^2, \tag{4.7}$$

thus proving that $\mathcal{H}_{sl}$ is equivalent to the biquadratic term suggested by Hayden *et al.*.

4.2 Strained Case

Based on the findings in [34], which state that it is the NN couplings that are affected the most under the influence of in–plane strain (see Section 3.1.1), simulations were performed. The parameter J_{ab} was changed from its assumed equilibrium value in Table 4.1 according to [34]. The results are shown in Fig. 4.5. Using this strain model, it is seen that compressive strain seems to drive the system towards the incommensurate spiral phase with wave vector $k_b = 0.46\pi$, while tensile strain further stabilizes the incommensurate E–type ordering. This can also be seen in Eq. (4.2), which verifies that smaller values of J_{ab}, i.e. tensile strain in the model used here, lessens the energy gain for the ab–spiral until eventually the E–type phase has lower energy. For very small values of the NN coupling, the correlation $\hat{S}_b$ gets weaker and a new peak appears for $k_b = 0.51\pi$. These peaks are, however, rather broad and it is not safe to draw definitive conclusions as to what precisely the $\hat{S}_b$ correlation is here. It is not clear from the literature what happens when the ratio J_{ab}/J_b goes to zero. It has been reported [30] that there is frustration in the lattice in the case $J_{ab}/J_b \ll 1, |J_a|/J_b \ll 1$, which is the state approached by the system with increasing tensile strain in the present model. In the same report, it is demonstrated that the sign of J_a becomes increasingly important with weaker NN couplings and it is stated that the present Heisenberg Hamiltonian, in which $J_a < 0$ is consistently used, breaks down and that $J_a > 0$ is correct instead. Hence, modeling tensile strain solely as an isotropic decrease in the absolute value of NN coupling might not be entirely justified, and the plot furthest to the back in Fig. 4.5 (colored green) may be inaccurate.

There exist several experimental works in which the effects of strain on $R\mathrm{MnO_3}$ have been investigated. Windsor *et al.* [2] study b–axis strain in epitaxially grown $\mathrm{LuMnO_3}$ films. Firstly, it is concluded, quite remarkably, that the peak wave vector of $\hat{S}_b$ locks in at $k_b \approx 0.485\pi$ for low temperatures, and then experiences a shift downward with increasing temperature. Also, greater amounts of (compressive) b–axis strain is demonstrated to increase this shift in the high–temperature region. This reported shift in the wave vector is, however, not observed in the present

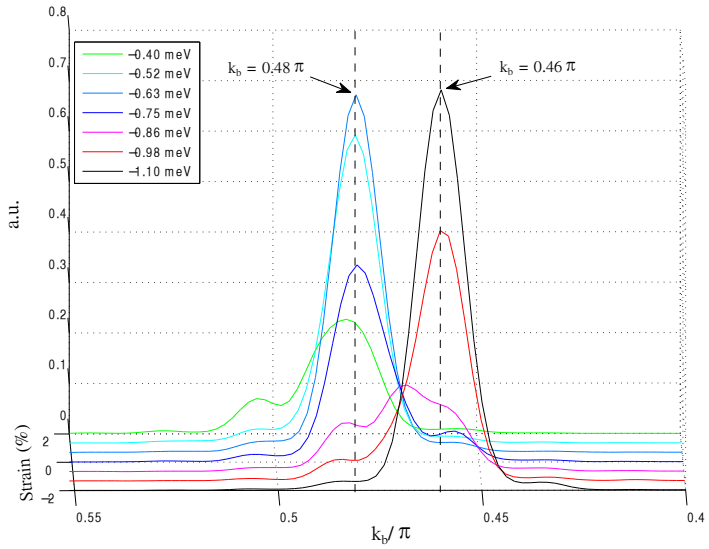

Figure 4.5: Peak values of the $\hat{S}_b$ correlation function when varying the J_{ab} parameter (see plot legend). Negative strains are compressive and positive strains are tensile. Here, $J_b = 4$ meV and $T = 1.4$ meV.

work; In some regions of the J_b–range, there is indeed a shift observed with increasing temperature. But it is not continuous and does not take place in the range reported by Windsor, but rather between the $k_b = 0.48\pi$ and $k_b = 0.46\pi$ peaks, which is attributed to the above–discussed coexistence between the incommensurate ab–spiral and E–type phases. Hence the reported effects of increasing compressive strain are absent in the present model.

Jiménez–Villacorta *et al.* [15] grow $YMnO_3$ epitaxial films on cubic single–crystal substrates and measure how the Mn–O–Mn bond angles and the anisotropic bond lengths due to lattice distortions change with film thickness (which in correlation with the amount of strain in the thin film). It is seen that the in–plane bond angles become larger with increasing strain, and that the antiferromagnetic order changes as a result of this, from spin–cycloidal ordering to A–type. In light of the present model, this corresponds to a shift to the left in Fig. 4.1 [9], which follows the same general trend as the present strain model observed through Fig. 4.5. It is stressed in [15], however, that an isotropic lattice–mismatch – which is the result of the cubic substrate used – does not create isotropic ab–plane strain in the $R\mathrm{MnO}_3$ structure, but rather the contrary. This indicates that the strain model in this work, in which the J_{ab} parameter was scaled isotropically, is inaccurate. The inclusion of anisotropic J_{ab} scaling is thus suggested as an outlook from this work.

Chapter 5

Summary and Conclusions

A Monte Carlo program has been constructed, which implements the Metropolis Algorithm to perform simulations of the magnetic phases of orthorombic manganese perovskites, $R\mathrm{MnO}_3$. A parallel tempering, replica exchange algorithm has been implemented so as to improve simulations in a cluster computer setting. A two–dimensional geometry was used, describing one ab–plane of the structure. An extended Heisenberg Hamiltonian was used to model the structure. In addition to the conventional nearest–neighbor and next–nearest–neighbor exchange couplings, terms were added so as to account for structural distortions which are fundamental to perovskite manganites and their magnetic structure:

$$\mathcal{H} = \mathcal{H}_{exc} + \mathcal{H}_{sl} + \mathcal{H}_{ani} + \mathcal{H}_{lat}, \tag{5.1}$$

where $\mathcal{H}_{exc}$ are the conventional Heisenberg exchange couplings, $\mathcal{H}_{sl}$ models the shifts of oxygen atoms in the Mn–O–Mn bonds due to octahedral tilting and Jahn–Teller distortions, $\mathcal{H}_{ani}$ is an anisotropy term which makes the c–axis a hard axis for the magnetization and $\mathcal{H}_{lat}$ is an elastic term which restores the forces on the oxygen atoms to equilibrium.

Simulations were performed on an equilibrium system so as to verify the Monte Carlo implementation and map results from the Hamiltonian (5.1) to previous existing results from simulations in a similar scheme. Phase transitions in the temperature domain agree rather well with what was previously reported (see Fig. 5.1). However, as expected, the present Hamiltonian cannot stabilize the two different kinds of incommensurate spin–cycloids that have been experimentally confirmed in the low–temperature region for certain $R\mathrm{MnO}_3$ compounds, and it is verified that the Dzyaloshinskii–Moriya interaction in combination with single–ion anisotropies is of great importance for establishing these kinds of ordering.

Also, phase evolutions which have been shown previously to occur when increasing the antiferromagnetic next–nearest–neighbor interaction, do so for much larger values than expected. This is attributed to the two–dimensional geometry and, again, to the absence of the DM interactions and sufficiently detailed anisotropy terms which fail to stabilize the bc–cycloid which would otherwise be an intermediary phase in–between the ab–spiral and E–type phases.

The anisotropy term in Eq. (5.1) affects the E–type phase which one expects to observe for large structural distortions. Without the anisotropy, the system is able to stabilize a commensurate E–type phase. But when adding even the weakest anisotropy, the system locks into an "incommensurate E–type phase", which agrees with experiments performed on thin films but not with results from bulk samples.

Attempts were then made to model strain in the $R\mathrm{MnO}_3$ structure within the Hamiltonian description in Eq. (5.1) and in accordance with previously reported experimental and theoretical results. Increasing compressive strain in the ab–plane affects the magnetic ordering in that a

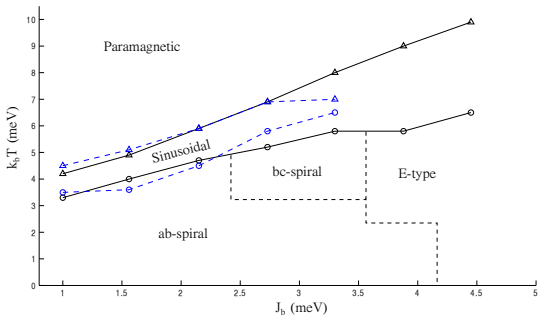

Figure 5.1: Reported phase diagram (black lines) as compared to previous results (blue lines).

compressively strained $R\mathrm{MnO}_3$ compound will achieve magnetic ordering similar to that of a compound with larger R radius. This is in accordance with previously reported experimental results. It is, however, valid within the present context only for small enough strains. For large strains, the model seems to break down. It is suggested that the inclusion of anisotropic ab–plane strains be investigated within the description in Eq. (5.1) as a possible outlook. Also, while the incommensurate E–type phase has been observed in the present model, the experimental reports of a shift in the incommensurate magnetic wave vector along the b–axis with increasing temperature for the E–type phase, and the claim that this shift increases with strain, have not. There is no clear consensus concerning the origins of this incommensurability in the E–type phase. And while there are many descriptions of how the $R\mathrm{MnO}_3$ structure changes under the influence of strain, no unified results exist to answer how the magnetic ordering might be affected, thus making phenomenological computer models such as that presented in this work a challenging task.

Bibliography

[1] T. Aoyama *et al.*, "Giant spin-driven ferroelectric polarization in $TbMnO_3$ under high pressure.", *Nat. Commun*, vol. 5, no. May, pp. 1–7, 2014.

[2] Y. W. Windsor *et al.*, "Multiferroic Properties of o–$LuMnO_3$ Controlled by b -Axis Strain", *Phys. Rev. Lett.*, vol. 113, no. 16, pp. 1–5, 2014.

[3] H. Schmid, "Multi-ferroic magnetoelectrics", *Ferroelectrics*, vol. 162, no. 1, pp. 317–338, 1994.

[4] B. B. Van Aken *et al.*, "Observation of ferrotoroidic domains.", *Nature*, vol. 449, no. 7163, pp. 702–705, 2007.

[5] S. Dong and J.-M. Liu, "Recent Progress of Multiferroic Perovskite Manganites", *Mod. Phys. Let. B*, vol. 26, no. 9, p. 1 230 004, 2012.

[6] T. Kimura *et al.*, "Magnetic control of ferroelectric polarization.", *Nature*, vol. 426, no. 6962, pp. 55–58, 2003.

[7] L. D. Landau, E. Lifshitz, *et al.*, *Electrodynamics of continuous media*. Elsevier, 1984, vol. 8.

[8] D. Khomskii, "Classifying multiferroics: Mechanisms and effects", *Physics*, vol. 2, 2009.

[9] M. Mochizuki *et al.*, "Theory of spin-phonon coupling in multiferroic manganese perovskites $RMnO_3$", *Phys. Rev. B*, vol. 84, pp. 1–14, 2011.

[10] S. Wall *et al.*, "Ultrafast coupling between light, Coherent lattice vibrations, and the magnetic structure of semicovalent $LaMnO_3$", *Phys. Rev. Lett.*, vol. 103, pp. 3–6, 2009.

[11] C. H. Marrows and B. J. Hickey, "New directions in spintronics.", *Philos. Trans. R. Soc. London, Ser. A*, vol. 369, no. 1948, pp. 3027–3036, 2011.

[12] M. Mochizuki *et al.*, "Spin model of magnetostrictions in multiferroic Mn perovskites", *Phys. Rev. Lett.*, vol. 105, pp. 1–4, 2010.

[13] M. E. Newman and G. T. Barkema, *Monte Carlo methods in statistical physics*. Oxford University Press, 1999.

[14] N. Locatelli, V. Cros, *et al.*, "Spin–torque building blocks", *Nature Materials*, vol. 13, no. 1, pp. 11–20, 2014.

[15] F. Jiménez-Villacorta *et al.*, "Strain-driven transition from E-type to A-type magnetic order in $YMnO_3$ epitaxial films", *Phys. Rev. B*, vol. 86, no. 2, pp. 1–4, 2012.

[16] M. Plischke and M. Bergersen, *Equilibrium statistical physics*, 3rd Ed. World Scientific, 2006.

[17] E. O. Wollan and W. C. Koehler, "Neutron Diffraction Study of the Magnetic Properties of the Series of Perovskite-Type Compounds [(1-x)La,xCa]MnO_3", *Phys. Rev.*, vol. 100, no. 2, pp. 545–563, 1955.

[18] R. J. Elliott, "Magnetic phase transitions", in *Magnetic Phase Transitions – Proceedings of a Summer School at the Ettore Majorana Centre, Erice, Italy*, M. Ausloos and R. J. Elliott, Eds., Springer–Verlag, 1983, pp. 2–24.

[19] H. F. Franzen, *Second-Order Phase Transitions and the Irreducible Representation of Space Groups*. Springer, 1982.

[20] E. Pavarini, "Crystal-field theory, tight-binding method and jahn-teller effect", in *Correlated electrons: from models to materials*, E. Pavarini, E. Koch, F. Anders, and M. Jarrell, Eds., vol. 2, Jülich: Forschungszentrum Jülich GmbH, 2012, ch. 6.

[21] M. C. M. O'Brien, "The Jahn–Teller effect: An introduction and current review", *Am. J. Phys.*, vol. 61, no. 1993, p. 688, 1993.

[22] M. Tachibana *et al.*, "Jahn-Teller distortion and magnetic transitions in perovskite $RMnO_3$ (R=Ho, Er, Tm, Yb, and Lu)", *Phys. Rev. B*, vol. 75, pp. 2–6, 2007.

[23] I. Solovyev *et al.*, "Crucial Role of the Lattice Distortion in the Magnetism of $LaMnO_3$", *Phys. Rev. Lett.*, vol. 76, no. 25, pp. 4825–4828, 1996.

[24] P. M. Woodward, "Octahedral Tilting in Perovskites. I. Geometrical Considerations", *Acta Crystallogr. Sec. B*, vol. 53, no. 1, pp. 32–43, 1997.

[25] ——, "Octahedral Tilting in Perovskites. II. Structure Stabilizing Forces", *Acta Crystallogr. Sec. B*, vol. 53, no. 1, pp. 44–66, 1997.

[26] E. Koch, "Exchange mechanisms", in *Correlated electrons: from models to materials*, E. Pavarini, E. Koch, F. Anders, and M. Jarrell, Eds., vol. 2, Jülich: Forschungszentrum Jülich GmbH, 2012, ch. 7.

[27] J. B. Goodenough, "An interpretation of the magnetic properties of the perovskite-type mixed crystals $La_{1-x}Sr_xCoO_{3-\lambda}$", *J. Phys. Chem. Solids*, vol. 6, no. 2, pp. 287–297, 1958.

[28] ——, "Theory of the role of covalence in the perovskite-type manganites [La,M(II)]MnO_3", *Phys. Rev.*, vol. 100, no. 2, pp. 564–573, 1955.

[29] J. Kanamori, "Superexchange interaction and symmetry properties of electron orbitals", *J. Phys. Chem. Solids*, vol. 10, no. 2-3, pp. 87–98, Jul. 1959.

[30] B. H. Kim and B. I. Min, "Nearest and next-nearest superexchange interactions in orthorhombic perovskite manganites $RMnO_3$ (R=rare earth)", *Phys. Rev. B*, vol. 80, no. 6, pp. 1–5, 2009.

[31] T. Kimura *et al.*, "Distorted Perovskite with e_g^1 Configuration as a Frustrated Spin System", *Phys. Rev. B*, vol. 68, p. 060 403, 2003.

[32] S. J. Blundell and K. M. Blundell, *Concepts in thermal physics*. Oxford University Press, 2010.

[33] W. Siemons *et al.*, "Strain dependence of transition temperatures and structural symmetry of $BiFeO_3$ within the tetragonal-like structure", *Appl. Phys. Lett.*, vol. 101, no. 2012, 2012.

[34] D. Iuşan *et al.*, "Effects of strain on ferroelectric polarization and magnetism in orthorhombic $HoMnO_3$", *Phys. Rev. B*, vol. 87, no. 1, pp. 1–8, 2013.

[35] N. Metropolis *et al.*, "Equation of State Calculations by Fast Computing Machines", *J. Chem. Phys.*, vol. 21, no. 1953, pp. 1087–1092, 1953.

[36] K. Hukushima and K. Nemoto, "Exchange Monte Carlo Method and Application to Spin Glass Simulations", *J. Phys. Soc. Jpn.*, vol. 65, pp. 1604–1608, 1996.

[37] Y. Li, M. Mascagni, and A. Gorin, "A decentralized parallel implementation for parallel tempering algorithm", *Parallel Computing*, vol. 35, no. 5, pp. 269–283, 2009.

[38] M. Mochizuki and N. Furukawa, "Microscopic model and phase diagrams of the multiferroic perovskite manganites", *Phys. Rev. B*, vol. 80, pp. 1–22, 2009.

[39] H. Okamoto *et al.*, "Neutron powder diffraction study of crystal and magnetic structures of orthorhombic $LuMnO_3$", *Solid State Commun.*, vol. 146, no. 3-4, pp. 152–156, 2008.

[40] N. S. Fedorova *et al.*, "Biquadratic and ring exchange interactions in orthorhombic perovskite manganites", *Phys. Rev. B*, vol. 91, no. 16, pp. 1–14, 2015.

[41] L. X. Hayden *et al.*, "Frustrated classical Heisenberg and XY models in two dimensions with nearest-neighbor biquadratic exchange: Exact solution for the ground-state phase diagram", *Phys. Rev. Lett.*, vol. 105, no. 4, pp. 1–4, 2010.

[42] T. A. Kaplan and S. D. Mahanti, 2009. arXiv:`0904.1739`.

[43] J. J. Sakurai and J. Napolitano, *Modern quantum mechanics*. Addison-Wesley, 2011.

[44] W. Fulton and J. Harris, *Representation Theory*. Springer, 1991.

[45] H. Anton and C. Rorres, *Elementary Linear Algebra: Applications Version*, 9th Ed. Wiley, 2005.

[46] M. I. Aroyo *et al.*, "Bilbao Crystallographic Server. II. Representations of crystallographic point groups and space groups", *Acta Crystallogr. Sec. A*, vol. 62, no. 2, pp. 115–128, Mar. 2006.

[47] A. P. Cracknell, "Group theory and magnetic phenomena in solids", *Rep. Prog. Phys.*, vol. 32, pp. 633–707, 1969.

[48] C. J. Bradley and B. L. Davies, "Magnetic groups and their corepresentations", *Rev. Mod. Phys.*, vol. 40, no. 2, pp. 359–379, 1968.

[49] J.-C. Tolédano and P. Tolédano, *The Landau Theory of Phase Transitions*. World Scientific, 1987.

[50] P. Tolédano, "Extensions and some recent applications of the Landau theory of phase transitions", in *Contribution of Symmetries in Condensed Matter*, V. Grenier, B and Simonet, Ed., vol. 22, 2012, pp. 1–38.

[51] A. B. Harris, "Landau analysis of the symmetry of the magnetic structure and magnetoelectric interaction in multiferroics", *Phys. Rev. B*, vol. 76, no. 5, 2007.

[52] P. Tolédano, "Magnetoelectric symmetry and the landau theory of phase transitions", *Ferroelectrics*, vol. 161, no. 1, pp. 257–273, 1994.

[53] R. Cowley, "Structural phase transitions I. Landau theory", *Adv. Phys.*, vol. 29, no. 1, pp. 1–110, 1980.

[54] A. Tröster *et al.*, "Fully consistent finite-strain landau theory for high-pressure phase transitions", *Phys. Rev. X*, vol. 4, no. 3, pp. 1–8, 2014.

[55] Y. Laosiritaworn and W. Laosiritaworn, "The Competition Effect of Strain and Interatomic Distance on Ferromagnetic Critical Temperature in Ising Ultra-Thin-Film: Monte Carlo Simulation", *Adv. Mat. Res.*, vol. 813, pp. 311–314, 2013.

[56] P. Tolédano, "Pseudo-proper ferroelectricity and magnetoelectric effects in $TbMnO_3$", *Phys. Rev. B*, vol. 79, no. January, pp. 2–5, 2009.

[57] L. C. Chapon *et al.*, "Helical magnetic state in the distorted triangular lattice of α-$CaCr_2O_4$", *Phys. Rev. B*, vol. 83, no. 2, pp. 1–6, 2011.

[58] M. Kenzelmann *et al.*, "Magnetic inversion symmetry breaking and ferroelectricity in $TbMnO_3$", *Phys. Rev. Lett.*, vol. 95, no. August, pp. 27–30, 2005.

Appendix A

Lattice Structure: Algebraic Description

Below follows an introduction to the algebraic treatment of magnetic ordering in lattices. Section A.1 introduces the fundamental concepts of representation theory which are needed in order to describe magnetic ordering using corepresentations, which is described in Section A.2. Together, these topics are important when working with Landau theory, which is presented in Appendix B.

A.1 Representation Theory

One way of working with a finite space group is to use *representations*, i.e. the homomorphic mapping of a set of (spatial) transformations onto a complex vector space. We define the representation of the group G as the finite–dimensional vector space V through the homomorphism ρ, given by

$$\rho : G \to GL(V). \tag{A.1}$$

Here, GL is a set of invertible (square) matrices of dimension $\dim(V)\times\dim(V)$. The homomorphism ρ can be seen as a projection of the space group G onto some subspace V and must be chosen wisely so as not to lose vital information of G. Eq. (A.1) describes how G, which is complicated in general, can be described by the representation V via the much simpler notion of square matrices GL. It remains, then, to classify V. In doing this, a few important results exist, which will be given here without proof (see [44] for a more detailed treatment):

1. A *subrepresentation* of a representation V is a vector subspace W of V which is invariant under G.
2. The representation V of the group G is called *irreducible* if there is no subrepresentations W of V other than 0 and V itself.
3. If V is a representation of the group G, and W is a subrepresentation of V (i.e. $W \subset V$), then there is a complementary subset $W' \subset V$ such that $V = W \oplus W'$.
4. *Schur's Lemma:* If V and W are irreducible representations (irreps) of G and $\phi : V \to W$ is a homomorphism on G, then
   a) Either ϕ is an isomorphism, or $\phi = 0$
   b) If $V = W$, then $\phi = \lambda \cdot I$ for some $\lambda \in \mathbb{C}$ and I the identity.

In other words, 1 and 2 simply say that there exist representations of the group G which cannot be decomposed into other, smaller representations. This in turn leads to 3, which states that each

reducible representation can be written as a tensor sum of a specific set of irreducible representations. Lastly, Schur's Lemma ascertains that each irrep of G is unique, up to isomorphism. This is a very important result, because it means that *every* representation V of the finite group G can be written as a sum of distinct irreps:

$$V = V_1^{\oplus a_1} \oplus \cdots \oplus V_k^{\oplus a_k}, \tag{A.2}$$

where $\{a_i\}$ are multiplicities. We have now reduced the problem of representing G to a matter of finding all irreps and then use them to decompose any representation of our chosing.

We are now in a position to find a way of decomposing representations into irreps. To do this, we make use of the *character* of a representation, which is defined as follows: Given an element $g \in G$, the character χ of g on the vector space V is given by

$$\chi_V(g) = \mathrm{Tr}(g_{|V}). \tag{A.3}$$

Noting also the well–established result from linear algebra that the trace of a matrix is invariant under any similarity transformation (see [45], for instance), we have that

$$\chi_V(hgh^{-1}) = \chi_V(g), \tag{A.4}$$

which means that there is a set of elements in G – a *conjugacy class* – which share a particular character. It follows, then, that the character of any representation V is a function of the characters of the conjugacy classes only, and thus we have simplified the problem even more. Using the arithmetic identities in Proposition 2.1 in [44], we can write the character of the representation (A.2) as a weighted sum of the characters of all the irreps of which the representation is composed:

$$\chi_V = a_1\chi_{V_1} + \cdots + a_k\chi_{V_k} \tag{A.5}$$

The results of such a treatment of a finite group can be summarized in a *character table* in which characters of all representations under all elements of the group are written. Table A.1 shows the character table of the crystallographic group *Pmmm* (or no. 47). The table uniquely determines the space group.

Table A.1: Character table of the point group of the crystallographic space group Pmmm (no. 47) [46]. The leftmost column shows the irreps, Γ^i. The first row shows the symmetry operations that make out the point group. Here, E is the identity, C_{ni} is a rotation by $\frac{2\pi}{n}$ about the i axis, σ_{ij} is a reflection in the ij–plane, S_n is rotoinversion ($S_n = \sigma_h \otimes C_n$). Lastly, $I = S_2$ is the inversion operator.

Pmmm	E	C_{2z}	C_{2y}	C_{2x}	I	σ_{xy}	σ_{xz}	σ_{yz}
Γ^{1+}	1	1	1	1	1	1	1	1
Γ^{2+}	1	1	-1	-1	1	1	-1	-1
Γ^{3+}	1	-1	-1	1	1	-1	-1	1
Γ^{4+}	1	-1	1	-1	1	-1	1	-1
Γ^{1-}	1	1	1	1	-1	-1	-1	-1
Γ^{2-}	1	1	1	1	-1	-1	1	1
Γ^{3-}	1	-1	-1	1	-1	1	1	-1
Γ^{4-}	1	-1	1	-1	-1	1	-1	1

A.2 Magnetic Groups and Corepresentations

Materials gain their magnetic properties due to the resultant effect of the magnetic moments of the atoms in the structure. Because of this, any space group used to describe a magnetic structure must also contain the antisymmetric operator (or, equivalently, the time reversal operator), $\mathcal{O}$. In fact, it can be shown [47] that the magnetic space groups must necessarily be on the form

$$M = G + \mathcal{O}G, \tag{A.6}$$

i.e. the magnetic groups are composed of a regular crystallographic space group and its product with $\mathcal{O}$ [48]. This way of constructing antiunitary groups from the unitary space groups creates a need for the framework of Section A.1 to be extended. Representation theory is no longer enough to fully describe the symmetries of magnetic structures. Rather, one must make use of *corepresentations*, which (luckily) resemble regular representations.

The first thing to note about the time reversal operator is that, given a wave function expanded in some basis, $|\psi\rangle = \sum_k a_k(t)\,|\psi_k\rangle$, it transforms as

$$\mathcal{O}\,|\psi\rangle = \sum_k a_k^*(t)\mathcal{O}\,|\psi_k\rangle\,, \tag{A.7}$$

where the asterisk denotes complex conjugation [47]. For reasons stated in Section A.1, it is convenient to use the irreps of a group as a basis for the state. Given a magnetic group M according to (A.6), representations of the unitary group G can be used such that, for all $R \in G$,

$$R\,\langle\psi_i| = \sum_{j=1}^{d} \langle\psi_j|\,\Delta(R)_{ji} = \langle\psi|\,\Delta(R), \tag{A.8}$$

where $\Delta(R)_{ji}$ are matrix elements of the unitary irrep of dimension d belonging to G [48]. (The last equality is shorthand notation.) The expression is written in accordance with the convention of left–action of operators on group elements [44]. This can now be expanded to account for the entire antiunitary group M by defining $\langle\gamma| = \langle\psi, \phi| = \langle\psi_1, \psi_2, \ldots, \psi_d, \phi_1, \phi_2, \ldots, \phi_d|$, where $\langle\phi| = \mathcal{O}\,\langle\psi|$. Now, according to Bradley [48], we write

$$R\,\langle\gamma| = \langle\gamma|\,D(R), \text{ where} \tag{A.9}$$

$$D(R) = \begin{pmatrix} \Delta(R) & 0 \\ 0 & \Delta^*(\mathcal{O}^{-1}R\mathcal{O}) \end{pmatrix}. \tag{A.10}$$

The matrix $D(R)$ is the *corepresentation* of R on M. Similarly, for all antiunitary elements $B \in \mathcal{O}G$, we have

$$B\,\langle\gamma| = \langle\gamma|\,D(B), \text{ where} \tag{A.11}$$

$$D(B) = \begin{pmatrix} 0 & \Delta(B\mathcal{O}) \\ \Delta^*(\mathcal{O}^{-1}B) & 0 \end{pmatrix}. \tag{A.12}$$

The corepresentations have properties similar to the regular representations in that there also exist *irreducible corepresentations* and that one can construct character tables. To describe all the possible magnetic symmetries available, one must include all symmetry operations R but also all antisymmetric operations $\mathcal{O}R$. Table A.2 shows an example.

An important application of the magnetic groups and (co–)representation theory exists within the framework of the Landau theory of phase transitions (see Appendix B).

Table A.2: Character table of the group Pca2$_1$1' at $\mathbf{k} = 0$. τ_i are the four corepresentations available and g_i are the (unitary) symmetry operations in the paramagnetic group [49].

$Pca2_11'$	g_1	g_2	g_3	g_4	$\mathcal{O}g_1$	$\mathcal{O}g_2$	$\mathcal{O}g_3$	$\mathcal{O}g_4$
τ_1	1	1	1	1	-1	-1	-1	-1
τ_2	1	1	-1	-1	-1	-1	1	1
τ_3	1	-1	1	-1	-1	1	-1	1
τ_4	1	-1	-1	1	-1	1	1	-1

Appendix B

Landau Theory

Landau theory has been an important aid in the study of phase transitions. It is successful in a great variety of scenarios: With very little prior knowledge about a system, one is able to draw general conclusions about symmetries and possible phases using Landau theory. If, on the other hand, one has more extensive knowledge about the system, accurate predictions may be made concerning the orders of the phase transitions and the temperatures at which they occur. This chapter describes the fundamental methodology. Also, the model is extended to account for strain influences and for the observed incommensurate phases appearing in most manganese perovskites.

B.1 Fundamentals

The temperature regime around a phase transition (magnetic or otherwise) is, by definition, non–equilibrium. Landau theory does, however, describe the situation from an equilibrium perspective, essentially by Taylor expanding the free energy, F, around the critical temperature, T_c. The idea is to express the free energy in terms of order parameters which leave invariant the free energy under the symmetry operations of the space groups in both phases [50]. Generally, lowering the temperature will induce phases with successively lower symmetry, and by *invariance*, it is meant that F does not change when applying symmetry operations of the paramagnetic group. The possible lower–symmetry phases will be subgroups of this parent group. Landau theory is useful in two main ways:

1. Given a paramagnetic space group, one is able to determine the possible ordered low–temperature phases and the order parameters describing the transition.

2. Given a known transition between two phases, one is able to determine its order.

It is here that the amount existing prior knowledge about the system comes into play. If one only knows the symmetry of the paramagnetic phase (the very minimum amount of information needed in order to be successful in applying the theory), then one can only list the possible low–temperature phases (and possibly the expected orders of transition). If no additional information is supplied, this is where the range of the theory ends – there is no way of knowing what phases will actually occur experimentally and what phases are mere theoretical constructions [49]. If, on the other hand, one does have experimental information about the phase(s), then the theory will be able to predict its nature and how it may be affected by distortions (strain, for instance) [51].

B.1.1 Symmetries

Table B.1 shows the symmetries of the paramagnetic group *Pnma* (No. 62), which matches the magnetic structure of the manganese perovskites. This describes the entire parent group, and given that the geometric structure itself does not change over the course of the transition, then all ordered symmetries will be subgroups of Pnma [52].

Table B.1: Character table of the group Pnma at $\mathbf{k} = 0$. Γ_i are the corepresentations available and g_i are the (unitary) symmetry operations in the paramagnetic group [46, 48].

Pnma	g_1	g_2	g_3	g_4	g_5	g_6	g_7	g_8
Γ_1^+	1	1	1	1	1	1	1	1
Γ_1^-	1	1	1	1	-1	-1	-1	-1
Γ_2^+	1	1	-1	-1	1	1	-1	-1
Γ_2^-	1	1	-1	-1	-1	-1	1	1
Γ_3^+	1	-1	-1	1	-1	1	1	-1
Γ_3^-	1	-1	-1	1	1	-1	-1	1
Γ_4^+	1	-1	1	-1	1	-1	1	-1
Γ_4^-	1	-1	1	-1	-1	1	-1	1
Pnma	$\mathcal{O}g_1$	$\mathcal{O}g_2$	$\mathcal{O}g_3$	$\mathcal{O}g_4$	$\mathcal{O}g_5$	$\mathcal{O}g_6$	$\mathcal{O}g_7$	$\mathcal{O}g_8$
Γ_1^+	-1	-1	-1	-1	-1	-1	-1	-1
Γ_1^-	-1	-1	-1	-1	1	1	1	1
Γ_2^+	-1	-1	1	1	-1	-1	1	1
Γ_2^-	-1	-1	1	1	1	1	-1	-1
Γ_3^+	-1	1	1	-1	1	-1	-1	1
Γ_3^-	-1	1	1	-1	-1	1	1	-1
Γ_4^+	-1	1	-1	1	-1	1	-1	1
Γ_4^-	-1	1	-1	1	1	-1	1	-1

Looking at Table B.1, we see that for any given corepresentation Γ_i, there is a unique set of symmetry operations g_i which leave the system invariant (i.e. whose characters are 1). For instance, the corepresentation Γ_2^+ is invariant under $g_1, g_2, g_5, g_6, \mathcal{O}g_3, \mathcal{O}g_4, \mathcal{O}g_7$ and $\mathcal{O}g_8$. This set of operations corresponds to a specific (antiferromagnetic) symmetry. Each corepresentation of a paramagnetic group thus corresponds to a possible ordered symmetry, and hence also a certain transition between two phases [49]. After deciding upon which corepresentation(s) of interest, one can construct the Landau free energy.

B.1.2 The Landau Free Energy

Generally, if a system can be described by an order parameter η (which, for example, could correspond to the total magnetization in a system), then the basic Landau free energy has the form

$$F(\eta, T) = F_0(T) + a\eta^2 + b\eta^4, \tag{B.1}$$

where F_0 is a background free energy, independent of η. Note how odd powers of η cannot be included in the expression since it would violate invariance under $\eta \to -\eta$, which would be unreasonable, at least in a magnetic system. One can then minimize F around $T = T_c$ by $\frac{\partial F(\eta, T_c)}{\partial \eta} = 0$ and $\frac{\partial^2 F(\eta, T_c)}{\partial \eta^2} = 0$. This is allowed because it is assumed that $\eta \to 0$ around T_c, something which

should always hold for any appropriate order parameter [16]. The fundamental result from Landau theory is that the coefficients a and b (and any higher–order coefficients, if present) determine the nature of the phase transition. They are often written $a = a_0(T - T_c)$ (and similarly for b). It turns out that a phase transition takes place when a or b changes sign. An important thing to note here is that *only one* of them may change sign [50].

After identifying a certain phase transition between two symmetries using the method in Section B.1.1, it remains to determine suitable order parameters which are left invariant under the transition. In the Pnma group there are 8 basis atoms (sub–lattices) corresponding to the 8 Mn atoms in the magnetic unit cell in the $R\mathrm{MnO}_3$ structure. If the spins are labeled $\{\vec{\mu}_i\}_{i=1}^{8}$, then one can form combinations of sublattice spins in accordance with the 8 corepresentations in Table B.1. Given a low–symmetry structure (i.e. a set of operations g_i), the structural invariance under these operations does not mean that all components of the $\vec{\mu}_i$ will also be invariant – the sublattice spin representations are *reducible*. It remains to find the components that *are* invariant, and it is these components that are suitable as order parameters [49].

As an example, we choose the $\mathrm{Pca2_11'}$ group, which has 4 basis atoms and is perhaps more instructive than the perovskite Pnma structure because it requires less lengthy expressions (they are, however, analogous in most respects). The $\mathrm{Pca2_11'}$ equivalent to Table B.1 is Table A.2, and one can construct four vectors from the different sublattices according to

$$\begin{aligned}
\mathbf{M} &= \vec{\mu}_1 + \vec{\mu}_2 + \vec{\mu}_3 + \vec{\mu}_4 \\
\mathbf{L_1} &= \vec{\mu}_1 + \vec{\mu}_2 - \vec{\mu}_3 - \vec{\mu}_4 \\
\mathbf{L_2} &= \vec{\mu}_1 - \vec{\mu}_2 + \vec{\mu}_3 - \vec{\mu}_4 \\
\mathbf{L_3} &= \vec{\mu}_1 - \vec{\mu}_2 - \vec{\mu}_3 + \vec{\mu}_4
\end{aligned}$$

(note how the signs match the characters corresponding to the four corepresentations in Table A.2). Similarly to Pnma, these are reducible since not all components of the $\vec{\mu}_i$ are invariant under the same symmetry operations. Those that are, however, are suitable order parameters in the Landau free energy. For τ_1 in Table A.2, for instance, it is L_{1z}, L_{2z} and L_{3y} that are invariant and parametrize the phase transition.

B.2 Strain Modeling

Magnetization and polarization are examples of *primary* order parameters, because they characterize the symmetry–breaking of the transition from high to low symmetry; They are invariant under all symmetry operations in both phases. There are, however, order parameters which do not obey all symetry operations, but still parametrize the Landau free energy around the phase transition. These are called *secondary* order parameters. One important use of secondary order parameters is to describe distortions which arise in the transition to the low–symmetry phase [53]. Hence, secondary order parameters are useful when studying the influences of strain in the ordered phases.

For temperature–driven transitions, and for relatively small applied strains, it is sufficient to treat the strains as infinitesimal (something which will also be relevant in Section B.2) [54]. Thus, one can define a linear strain tensor

$$\epsilon_{ij} = \frac{r_0^{ij} - r_0}{r_0}, \tag{B.2}$$

where r_0 is the equilibrium position and r_0^{ij} is the deviation from it in the ij direction ($i = j$ signifies a deviation along an axis and $i \neq j$ is a deviation perpendicular to the ij–plane). ϵ_{ij} is

taken into account in the Landau free energy (B.1) by adding first a *coupling invariant* term and then an elastic term [49]. If, for instance, the strain is taken to be in one direction only, then Eq. (B.1) will be extended as follows:

$$F(\eta, T) = F_0(\eta) + a\eta^2 + b\eta^4 + c\eta^2\epsilon_{ii} + \frac{1}{2}C\epsilon_{ii}^2, \tag{B.3}$$

where the last two terms are the coupling invariant and elastic term, respectively. When minimizing the above with respect to ϵ_{ii}, one can identify the equilibrium strain and reinsert it into Eq. (B.3). By doing this, one will have renormalized $F(\eta, T)$ in the η^4 term, and it is seen that the strain influences the stability of the phase [50].

It is worth mentioning that arguments have been raised that infinitesimal strain models such as the above are used all too incautiously, and that they are inaccurate in describing anything other than pure temperature–driven transitions [54]. Attempts have been made to increase the accuracy of the model by going beyond harmonic order in the free energy [54, 55]. In this work, however, only infinitesimal strains are considered, and so the elastic model presented above is justified.

B.3 Incommensurate Phases

Incommensurate (IC) phases have larger unit cells than the paramagnetic group, and hence the symmetry arguments presented in the previous section must be extended so as to account for a non–zero wave vector in the Brillouin zone. First of all, by definition, it is not possible to describe IC structures using a magnetic space group [50], because periodic translations of the paramagnetic unit cell do not exist in the IC magnetic context. Instead, only the magnetic point group is used. Generally, an IC order parameter can be written $S = S_0 e^{i\mathbf{k}\cdot\mathbf{r}}$, where $\mathbf{k}$ is the modulation vector in reciprocal space. Again, depending on the knowledge beforehand about the system that is to be described, the Landau theory can be used in different ways.

Table B.2: Generators of the irreducible corepresentations Δ_2 and Δ_3 of the paramagnetic group Pbnm1' (see text) [56, 57]. The order parameters S_2 and S_3 (and their complex conjugates) transform according to the matrices in the table. Here, ϵ is connected to the wave vector of the phase of interest (be it IC or not).

Pbnm1'		$(U_y\|\frac{a}{2}\frac{b}{2}0)$	$(\sigma_z\|00\frac{c}{2})$	$(I\|000)$	$\mathcal{C}$	$(E\|0b0)$
Δ_2	S_2 S_2^*	$\begin{pmatrix} e^{i\epsilon} & 0 \\ 0 & e^{-i\epsilon} \end{pmatrix}$	$\begin{pmatrix} -1 & 0 \\ 0 & -1 \end{pmatrix}$	$\begin{pmatrix} 0 & 1 \\ 1 & 0 \end{pmatrix}$	$\begin{pmatrix} -1 & 0 \\ 0 & -1 \end{pmatrix}$	$\begin{pmatrix} e^{2i\epsilon} & 0 \\ 0 & e^{-2i\epsilon} \end{pmatrix}$
Δ_3	S_3 S_3^*	$\begin{pmatrix} -e^{i\epsilon} & 0 \\ 0 & -e^{-i\epsilon} \end{pmatrix}$	$\begin{pmatrix} 1 & 0 \\ 0 & 1 \end{pmatrix}$	$\begin{pmatrix} 0 & 1 \\ 1 & 0 \end{pmatrix}$	$\begin{pmatrix} -1 & 0 \\ 0 & -1 \end{pmatrix}$	$\begin{pmatrix} e^{2i\epsilon} & 0 \\ 0 & e^{-2i\epsilon} \end{pmatrix}$

For example, in the case of lanthanide perovskite manganites (RMnO$_3$ with R=La–Lu), it has been observed [57, 58] that, out of four possible corepresentations in the Pbnm space group (which, in addition to the Pnma group, can be used to describe orthorombic perovskites), two are responsible for the symmetry–breaking transitions, labeled Δ_2 and Δ_3, the character table of which is seen in Table B.2. Using this knowledge, one can define order parameter invariants which characterize the transitions

$$\mathcal{J}_1 = S_2^2 \tag{B.4}$$

$$\mathcal{J}_2 = S_3^2 \tag{B.5}$$

$$\mathcal{J}_3 = S_2^2 S_3^2 \cos 2\phi. \tag{B.6}$$

Here, the order parameters are defined using $S_2 = S_2^0 e^{i\theta_2}, S_2^* = S_2^0 e^{-i\theta_2}, S_3 = S_3^0 e^{i\theta_3}$ and $S_3^* = S_3^0 e^{-i\theta_3}$ which are the complex amplitudes transforming according to Δ_2 and Δ_3, respectively. The mixing phase angle is $\phi = \theta_2 - \theta_3$. The free energy can then be written as [56]

$$F(S_2, S_3, \phi, T) = F_0(T) + \sum_{i=1}^{2} \left[\frac{\alpha_i}{2} \mathcal{J}_i + \frac{\beta_i}{4} \mathcal{J}_i^2 \right] + \frac{\gamma_1}{2} \mathcal{J}_3 + \frac{\gamma_2}{2} \mathcal{J}_3^2 + \dots . \tag{B.7}$$

When minimizing with respect to the parameters S_2, S_3 and ϕ, one gets five different stable states, corresponding to different values of the complex amplitudes and the mixing angle [50, 56]. Two of these are the sinusoidal and E–type ordered states reported in the literature (e.g. by [5, 6, 9, 30]). Using knowledge (experimental or theoretical) of the wave vectors of these two states, one can replace ϵ in the character table B.2 with real values and analyze, for instance, the orders of the transitions.

TRITA ICT-EX-2015:43